AD-A045 215 UNITED TECHNOLOGIES RESEARCH CENTER EAST HARTFORD CONN F/G 20/5
ANALYSIS OF THE FACTORS CAUSING GLOW COLLAPSE IN HIGH ENERGY EL--ETC(U)
JUL 77 W L NIGHAN, W J WIEGAND , R J HALL F33615-76-C-2046
UNCLASSIFIED UTRC/R77-922295-5 AFAPL-TR-77-34 NL

1 OF 1
ADA
045215

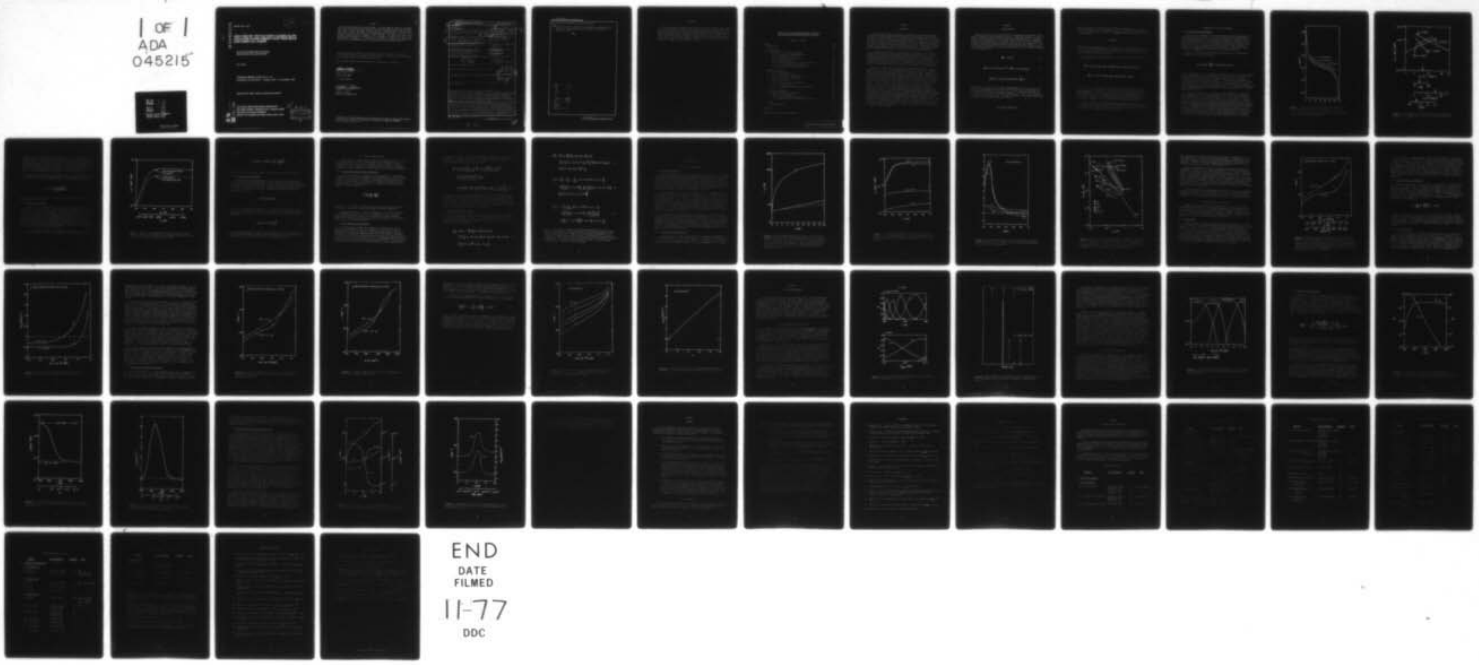

END
DATE
FILMED
11-77
DDC

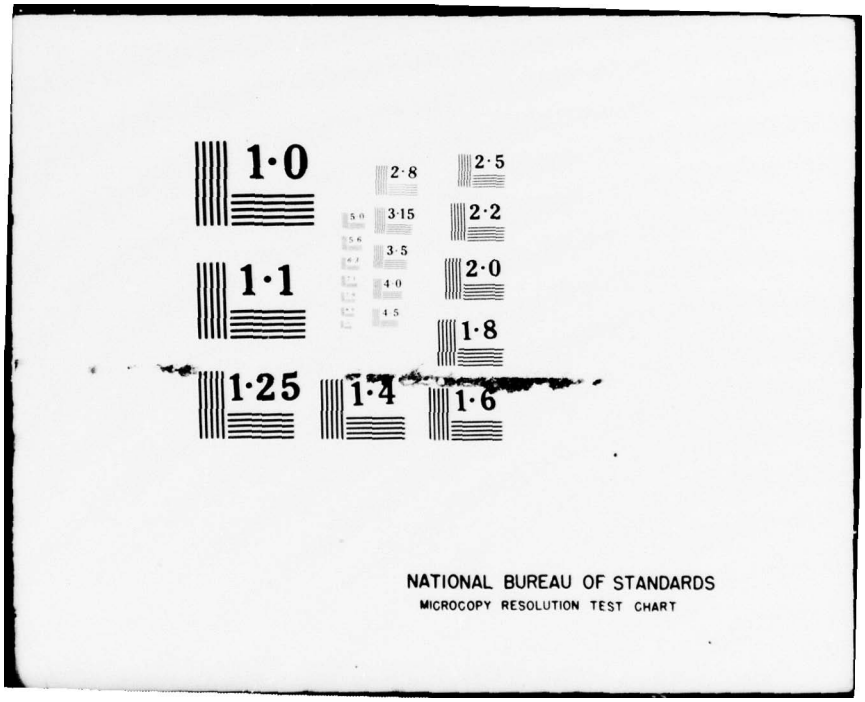
1·0
1·1
1·25
1·4
1·6
1·8
2·0
2·2
2·5
2·8
3·15
3·5
4·0
4·5
5·0
5·6
NATIONAL BUREAU OF STANDARDS
MICROCOPY RESOLUTION TEST CHART

AFAPL-TR-77-34

ANALYSIS OF THE FACTORS CAUSING GLOW COLLAPSE IN HIGH ENERGY ELECTRON BEAM SUSTAINED CO LASERS

United Technologies Research Center
East Hartford, Connecticut 06108

July 1977

TECHNICAL REPORT AFAPL-TR-77-34
Final Report for the Period 1 January 1976 - 31 December 1976

AIR FORCE AERO-PROPULSION LABORATORY
AIR FORCE WRIGHT AERONAUTICAL LABORATORIES
AIR FORCE SYSTEMS COMMAND
WRIGHT-PATTERSON AIR FORCE BASE, OHIO 45433

NOTICE

When Government drawings, specifications, or other data are used for any purpose other than in connection with a definitely related Government procurement operation, the United States Government thereby incurs no responsibility nor any obligation whatsoever; and the fact that the government may have formulated, furnished, or in any way supplied the said drawings, specifications, or other data, is not to be regarded by implication or otherwise as in any manner licensing the holder or any other person or corporation, or conveying any rights or permission to manufacture, use, or sell any patented invention that may in any way be related thereto.

This report has been reviewed by the Information Office (IO) and is releasable to the National Technical Information Service (NTIS). At NTIS, it will be available to the general public, including foreign nations.

This technical report has been reviewed and is approved for publication.

William F. Bailey

William F. Bailey
Major, USAF
Project Engineer

FOR THE COMMANDER

Philip E Stover

Signature and Title

PHILIP E. STOVER
Chief, High Power Branch

Copies of this report should not be returned unless return is required by security considerations, contractual obligations, or notice on a specific document.

UNCLASSIFIED

SECURITY CLASSIFICATION OF THIS PAGE (When Data Entered)

REPORT DOCUMENTATION PAGE

READ INSTRUCTIONS BEFORE COMPLETING FORM

1. REPORT NUMBER: AFAPL-TR-77-34	2. GOVT ACCESSION NO.
3. RECIPIENT'S CATALOG NUMBER	
4. TITLE (and Subtitle): ANALYSIS OF THE FACTORS CAUSING GLOW COLLAPSE IN HIGH ENERGY ELECTRON BEAM SUSTAINED CO LASERS	5. TYPE OF REPORT & PERIOD COVERED: Final Report. Jan. 1, 1976 - Dec. 31, 1976
	6. PERFORMING ORG. REPORT NUMBER: R77-922295-5
7. AUTHOR(s): William L. Nighan, Walter J. Wiegand, Robert J. Hall and Robert H. Bullis	8. CONTRACT OR GRANT NUMBER(s): F33615-76-C-2046
9. PERFORMING ORGANIZATION NAME AND ADDRESS: United Technologies Research Center, Silver Lane, East Hartford, Connecticut 06108	10. PROGRAM ELEMENT, PROJECT, TASK AREA & WORK UNIT NUMBERS: Project 7073, Task 2301-S2, Work Unit 16
11. CONTROLLING OFFICE NAME AND ADDRESS: Air Force Aero Propulsion Laboratory, Air Force Systems Command, Wright-Patterson AFB, OH 45433	12. REPORT DATE: July 1977
	13. NUMBER OF PAGES: 52
14. MONITORING AGENCY NAME & ADDRESS (if different from Controlling Office)	15. SECURITY CLASS. (of this report): Unclassified
	15a. DECLASSIFICATION DOWNGRADING SCHEDULE

16. DISTRIBUTION STATEMENT (of this Report)

Approved for public release; distribution unlimited

DDC RECEIVED OCT 14 1977 B

17. DISTRIBUTION STATEMENT (of the abstract entered in Block 20, if different from Report)

18. SUPPLEMENTARY NOTES

19. KEY WORDS (Continue on reverse side if necessary and identify by block number)

High Energy CO Lasers, Plasma Instability in Lasers, Externally Sustained Laser Stability, CO Electric Lasers, Stability of Convection Lasers, Stability of Electron-Beam Ionized Lasers, Ion Species in Laser Discharges, Positive Ion Chemistry in High Pressure Discharges, Hydrated-Hydronium Ions in Discharges,

20. ABSTRACT (Continue on reverse side if necessary and identify by block number)

In this investigation the causes of thermal instability in high power CO laser discharges were examined. This analysis showed that externally sustained CO laser discharges are inherently unstable, having instability-growth times on the order of 0.1 msec. The single most important factor affecting instability growth at a specific power density level was found to be electron-positive ion recombination. Changes in the recombination process as a consequence of positive ion kinetics were found to result in order of magnitude variations in →

DD FORM 1 JAN 73 1473 EDITION OF 1 NOV 65 IS OBSOLETE

Unclassified

SECURITY CLASSIFICATION OF THIS PAGE (When Data Entered)

409252

19. Cluster-Ion Recombination in Laser Discharges.

20. instability growth. Because of the importance of recombination the effects of ion clustering reactions and water-ion chemistry are discussed in detail.

FOREWORD

This final report was submitted by United Technologies Research Center (UTRC), under Contract F33615-76-C-2046. The effort was sponsored by the Air Force Aero Propulsion Laboratory, Air Force Systems Command, Wright-Patterson AFB, Ohio under Project 7073, Task 2301-S2 and Work Unit 16 with Major William F. Bailey POP, Project Engineer In-Charge. William L. Nighan of UTRC was technically responsible for the work; other UTRC staff members contributing to the program were Walter J. Wiegand, Jr., Robert J. Hall and Robert H. Bullis.

Analysis of The Factors Causing Glow Collapse in
High Energy Electron Beam Sustained CO Lasers

TABLE OF CONTENTS

SECTION 1

INTRODUCTION

The maximum power density attainable in externally sustained molecular laser discharges is usually dictated by the occurrence of glow collapse and/or arcing. The erratic and unpredictable nature of this phenomenon severely hinders the development of large scale, high power electric laser systems. In a previous investigation[1] the causes of thermal instability in externally sustained discharges were analyzed for conditions typical of cw, convection cooled CO_2 lasers. It was found that such discharges are thermally unstable and that the magnitude of the instability growth rate is exceptionally sensitive to the nature of the electron loss process.

In the present investigation a similar analysis is applied to high energy CO electric laser discharges. The primary objectives of this study are: (1) identification of the physical mechanisms from which instabilities arise for low temperature-high pressure CO laser operating conditions; and (2) identification of the plasma properties which impact on the development of thermal instabilities. The information so generated should assist in identification of means to extend and/or enhance the stable operating range of externally controlled CO laser discharges.

Most of the details of the theoretical formulation used have been reported previously.[1-4] In Sec. 2 those specific features which are unique to CO electric lasers are treated, particularly, vibrational-translational energy relaxation under conditions such that the vibrational energy distribution is highly nonBoltzmann; and electron-molecule super-elastic collisions which are important when a significant fraction of the molecules are vibrationally excited. A very brief review of the linear stability model used in this analysis is also presented. Thermal instability growth in CO lasers and the factors influencing this phenomenon are presented in detail in Sec. 3. There it is shown that changes in the nature of electron-ion recombination greatly influence the magnitude of the instability growth rate. Because of the importance of recombination, positive ion chemistry is discussed in some detail in Sec. 4. On the basis of available experimental data related to ion identification in high pressure gases it is argued that positive ion species typical of CO laser conditions will be clustered, and that the ion species will be dominated by impurities in the gas mixture, especially water molecules. In view of the importance of the electron loss process on thermal instability growth, and the myriad of factors affecting cluster ion recombination in a vibrationally active gas, this conclusion is of particular importance. Indeed, on the basis of this study the need for a greatly improved understanding of cluster ion production and loss mechanisms in discharges becomes apparent.

SECTION 2

PLASMA ANALYSIS

Rigorous formulation of the criteria for the occurrence of instability in gas mixtures containing several molecular species is a formidable problem. In order to retain a manageable analytical model it has been assumed that the only molecular species in the discharge is CO in an atomic diluent such as He or Ar. Rotational-translational equilibrium has been assumed to exist at the gas temperature, T. The resulting conservation equations for the neutral particle number density and the translational-rotational and vibrational energy densities for a convection discharge are then expressed,[1,2,4]

$$\frac{Dn}{Dt} + n \nabla \cdot \underset{\sim}{U} = 0 , \tag{1}$$

$$\frac{D}{Dt}(n\varepsilon_T) + (n\varepsilon_T + P)\nabla \cdot \underset{\sim}{U} = \kappa \nabla^2 T + \frac{n_m}{\tau_{VT}} \varepsilon_V + n_e n (\nu_T/n) k T_e \quad , \tag{2}$$

$$\frac{D}{Dt}(n_m \varepsilon_v) + n_m \varepsilon_v \nabla \cdot \underset{\sim}{U} = n_e n (\nu_v/n) k T_e - \frac{n_m}{\tau_{VT}} \varepsilon_V \quad , \tag{3}$$

where $D/Dt = \partial/\partial t + \underset{\sim}{U} \cdot \nabla$, U is the mass average velocity of the gas, n and n_m are the total neutral particle number density and molecule density, respectively, κ is the thermal conductivity of the gas, and τ_{VT} is the temperature dependent time characterizing vibrational-translational relaxation, i.e., $\tau_{VT}^{-1} = nk_{VT}$, with k_{VT} the effective rate coefficient for V-T energy relaxation. The average translational-rotational energy per particle, ε_T, is given by,

$$\varepsilon_T = (3/2\ x_a + 5/2\ x_m) kT \quad ,$$

where X_a and X_m are the atom and molecule fractional concentrations. In order to facilitate comparison with the formulation of Ref. 1, the average vibrational energy per CO molecule, $\mathcal{E}_V$, will be related to an effective vibrational temperature defined by the expression,

$$\mathcal{E}_V \equiv kT_V .$$

Regarding the electron properties in Eqs. (1)-(3), n_e is the electron density, T_e is the generalized (nonBoltzmann) electron temperature [2,3], and ν_V and ν_T are the electron temperature dependent collision frequencies for vibrational excitation and gas translational heating, respectively.

The corresponding particle conservation equations for electrons and negative ions are written,[4]

$$\frac{Dn_e}{Dt} + n_e \nabla \cdot \underset{\sim}{U} + \nabla \cdot (n_e \underset{\sim}{U}_e) = n_e n k_i - n_e n_p k_r^e - n_e n k_{a_1} - n_e n^2 k_{a_2} + n_n n k_d + n S_E , \quad (4)$$

$$\frac{Dn_n}{Dt} + n_n \nabla \cdot \underset{\sim}{U} + \nabla \cdot (n_n \underset{\sim}{U}_n) = n_e n k_{a_1} + n_e n^2 k_{a_2} - n_n n_p k_r^i - n_n n k_d , \quad (5)$$

where n_n and n_p are the negative ion and positive ion number densities ($n_p = n_e + n_n$), U_e and U_n are the electron and negative ion drift velocities, and the indicated mixture weighted rate coefficients are those for single step ionization by low energy electrons (k_i), electron recombination (k_r^e), dissociative attachment (k_{a_1}), three-body attachment (k_{a_2}), detachment (k_d), and ion-ion recombination (k_r^i). The quantity S_E represents the electron production rate due to the external source of ionization; generally $nS_E \gg n_e n k_i$ for the conditions of primary interest.

Detailed discussions of the approximations and formulation leading to Eqs. (1)-(5) as applied to this problem are presented elsewhere.[1-4] Also, the specific features of the charged particle collision processes represented in Eqs. (4) and (5), have been discussed in considerable detail in Refs. 3 and 5.

2.1 Application to CO Laser Discharges

2.1.1 Vibrational Energy Relaxation

Probably the most important feature distinguishing CO electric discharge lasers from otherwise similar CO_2 lasers is the highly nonBoltzmann vibrational energy distribution characteristic of the anharmonic pumping effect.[6] Although the form of the vibrational energy distribution changes in response to variations in any of the variables T_e, n_e, T and n, V-V energy exchange processes are sufficiently fast ($\lesssim 10^{-6}$ sec) so that the vibrational distribution can be assumed to respond to disturbances in plasma properties in a quasisteady fashion. This permits determination of an effective rate coefficient for V-T energy relaxation.

Equation (3) shows that the vibrational power balance for a uniform steady state plasma can be written in the form,

$$n_e n(\nu_v/n)kT_e = \frac{n_{co}\varepsilon_v}{\tau_{VT}} = n_{co} n k_{VT}(T_e, n_e, T, n)kT_v \quad , \tag{6}$$

where the dependence of the V-T relaxation coefficient on T_e, n_e, T, and n is indicated. In order to determine the rate coefficient k_{VT} as defined by Eq. (6), steady state CO vibrational energy distributions and energy transfer rates were determined numerically using a molecular kinetics model.[6] A CO:He mixture in the proportions 0.1:0.9 was used; and the ranges of variables covered were: T, 50-100°K; n_e, 2×10^{11} -2×10^{12} cm^{-3}; P, 50-200 torr; and T_e, 0.4-1.5 eV. These properties correspond to electrical power densities in the 50-2000 Wcm^{-3} range. For the purpose of illustration, computed vibrational population distributions for conditions typical of this analysis are presented in Fig. 1.

In order to assess the effect of changes in plasma properties on vibrational energy relaxation, each of the variables T_e, n_e, T and n was varied independently about the following base (or reference) values: T_{e_o} = 0.56 eV (i.e., $E/n = 1.0 \times 10^{-16}$ Vcm^2); $n_{e_o} = 7.5 \times 10^{11}$ cm^{-3}; T_o = 65°K and $n_o = 1.48 \times 10^{19}$ cm^{-3}. Numerical evaluation of the steady state CO vibrational energy distributions and the corresponding vibrational energy density, ε_v, then permitted determination of k_{VT} as defined by Eq. (6). Effective V-T rate coefficient data obtained on this basis are presented in Fig. 2. Examination of this figure shows that k_{VT} increases with both T_e and n_e. This reflects the fact that as the amount of vibrational excitation increases, the anharmonic pumping effect drives energy to higher vibrational levels from which V-V-T and V-T relaxation is more effective. As the neutral number density is increased the energy stored in vibration per molecule simply decreases with a corresponding

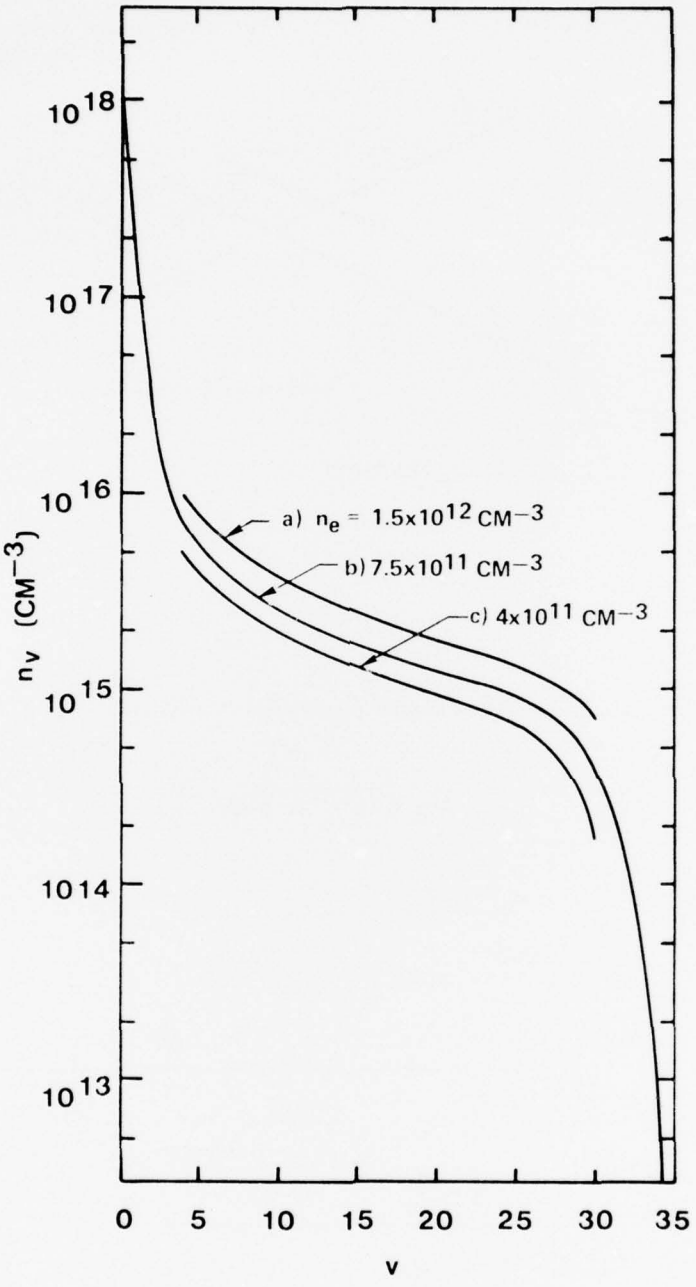

Figure 1. CO vibrational population distributions computed for a CO-He(0.1:0.9) mixture and the base conditions: T_o = 65°K, n_o= 1.48 x 10^{19} cm^{-3}, $(E/n)_o$ = 1.0 x 10^{-16} V cm^2 (T_e ≃ 0.56 eV): the effective vibrational temperatures corresponding to curves a-c are 2360°K, 1800°K and 1340°K, respectively.

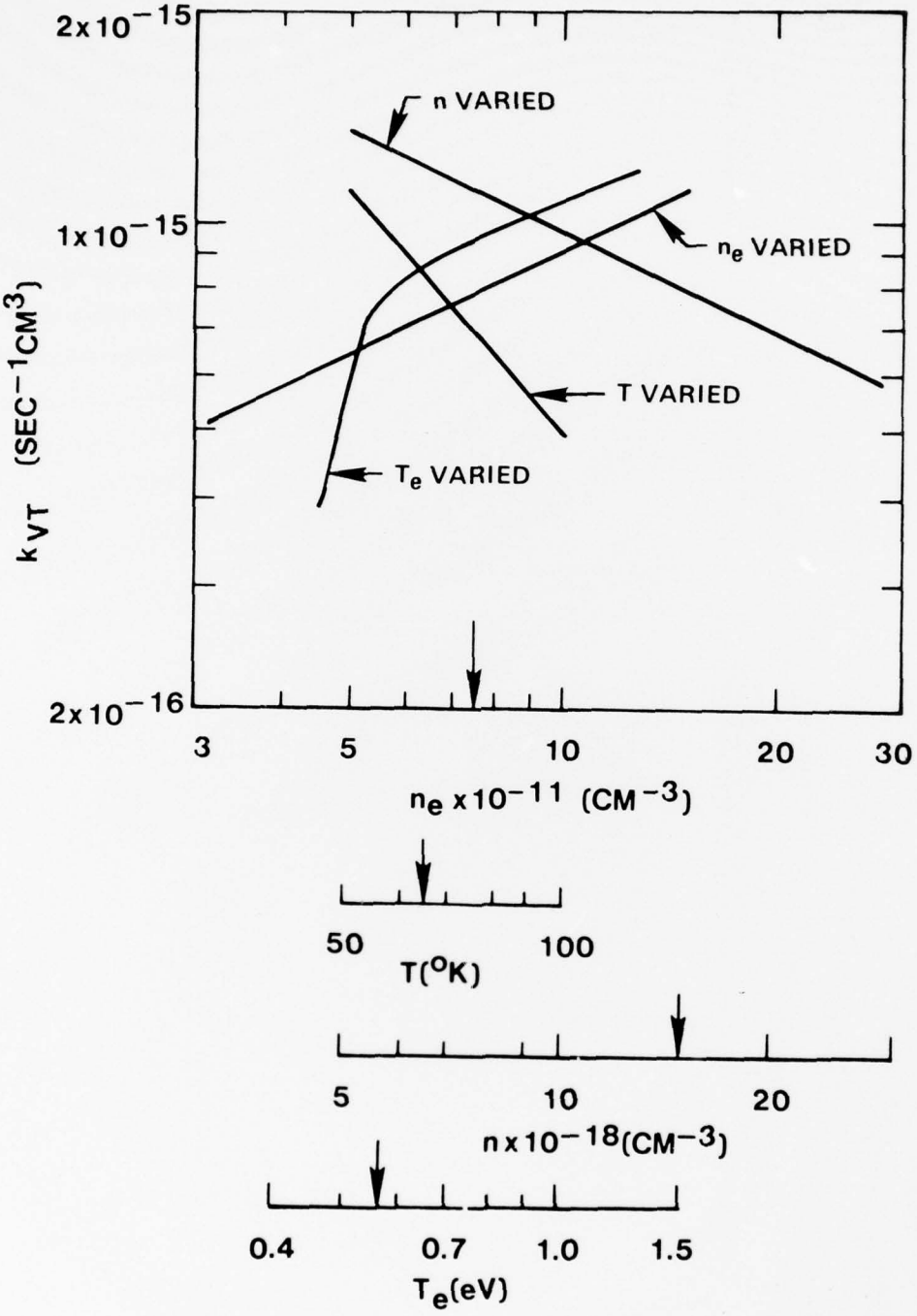

Figure 2. Computed variation of the effective V-T energy transfer coefficient for a CO-He (0.1:0.9) mixture. Reference conditions are indicated by the arrows.

decrease in vibrational relaxation. Of particular interest is the fact that as the gas temperature is increased, anharmonic pumping of energy to higher levels is less effective, leading to a decrease in the vibrational relaxation rate coefficient. At much higher temperatures k_{VT} ultimately tends toward the Landau-Teller value, $k_{VT}(T) \cdot (1-\exp(-\epsilon/kT))^{-1}$, as $\mathcal{E}_v$ tends toward a Boltzmann distribution. Under certain conditions such a negative temperature dependence of $k_{VT}(T)$ could have a significant effect on thermal stability since an increase in T results in a decrease in the effective vibrational relaxation rate coefficient, i.e., negative feedback.

The k_{VT} data presented in Fig. 2 are found to exhibit a monotonic dependence on the variables n_e, T and n. Therefore, application of perturbation theory to Eqs. (1)-(3) can be simplifed by expressing the V-T rate coefficient in the form,

$$k_{VT} = k_{VT}(T_e)\left(\frac{n_e}{n_{e_o}}\right)^{\alpha}\left(\frac{T}{T_o}\right)^{\beta}\left(\frac{n}{n_o}\right)^{\gamma} . \qquad (7)$$

The values $\alpha = 0.5$, $\beta = -1.15$ and $\gamma = -0.5$ are found to yield a very good fit to the numerical data shown in Fig. 2.

2.1.2 Superelastic Collisions

In addition to its usual dependence on T_e, the electron vibrational excitation coefficient, ν_v/n, also depends on n_e, T and n because of their impact on T_v. As T_v increases ν_v/n is reduced as a consequence of electron-molecule superelastic collisions. On the basis of numerical experimentation it was found that within the range of variables described previously, the dependence of the vibrational excitation coefficient on changes in n_e, T and n was relatively weak. However, the effect of superelastic collisions on ν_v/n as T_e is varied was found to be much more pronounced, reflecting the highly nonlinear dependence of vibrational excitation on electron energy. The data presented in Fig. 3 show the resulting effect on ν_v/n of variations in T_e. The values of effective vibrational temperature corresponding to the reference values of n_e, T and n are also given in the figure.

In order to simplify formulation of the stability analysis, the rate coefficient data of Fig. 3 (including superelastic collisions) have been approximated by the

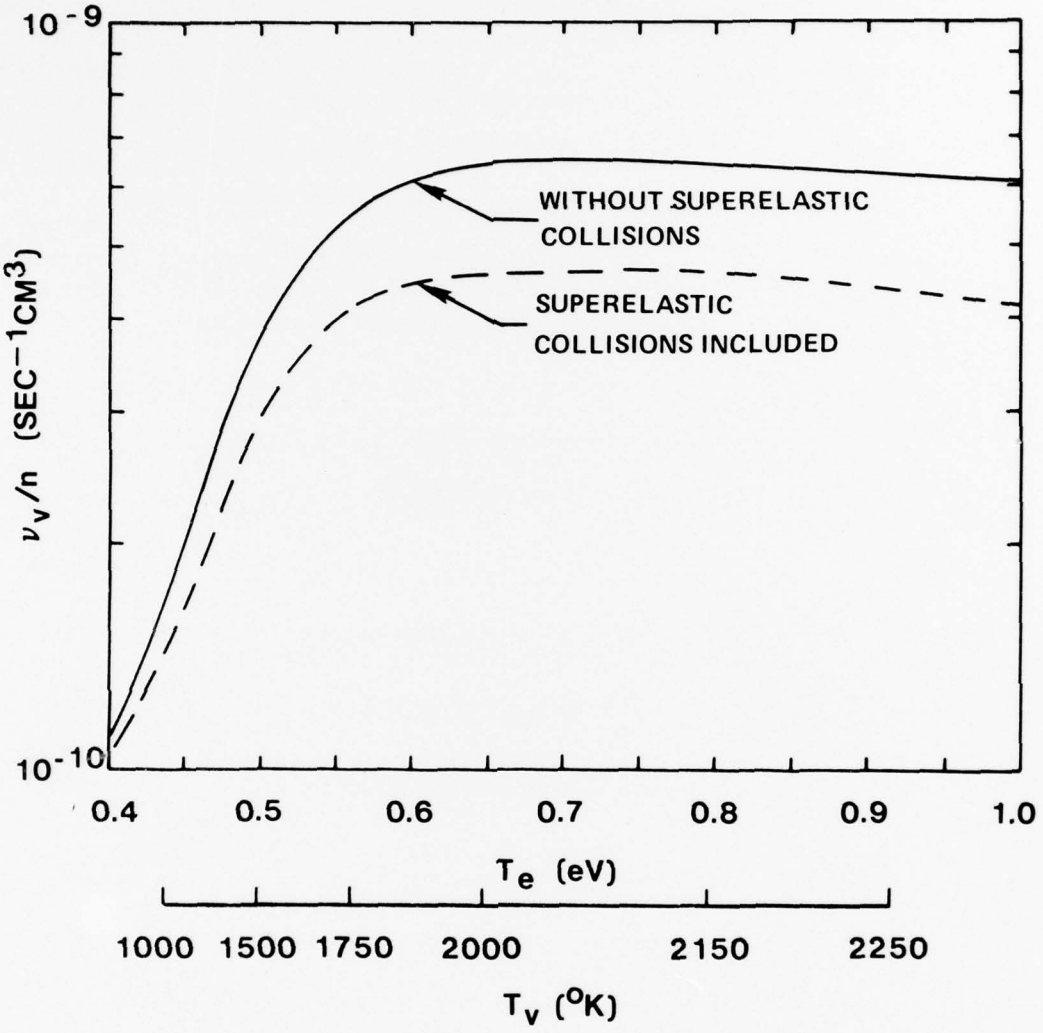

Figure 3. Computed electron-molecule vibrational excitation coefficient in a CO-He (0.1:0.9) mixture at the reference conditions with and without the influence of superelastic collisions.

expression,

$$\nu_V(T_e,T_v)/n = (\nu_v(T_e)/n)_o \left[1-\left(\frac{T_v}{10^4}\right)^{\zeta}\right] , \tag{8}$$

where $\zeta = 0.8$ has been found to yield a very good fit to the numerical results.

2.1.3 Electron-Ion Recombination

For high pressure-low temperature conditions positive ion species will be clustered [7-9] with the likelihood that no single species of ion dominates over the entire range of conditions encountered. Further, the magnitude of the recombination coefficient of clustered ions can vary significantly, even among members of the same family.[9] Therefore the effective recombination coefficient k_r^e should be expressed in the form,

$$k_r^e = \sum_j f_j(T) k_{r_j}^e (T_e) , \tag{9}$$

where f_j is the fractional concentration of the j^{th} ion species and $k_{r_j}^e$ is the corresponding recombination coefficient. By assuming that the electron temperature dependence of the various ion species is the same k_r^e can be approximated by the expression,

$$k_r^e (T_e,T) = k_r^e (T_e)\left(\frac{T}{T_c}\right)^{\delta} . \tag{10}$$

In the numerical analysis to follow T_o has been taken as 65^oK and the exponent δ has been varied parametrically. Sections 3 and 4 treat the matter of electron recombination for CO (and CO_2) laser conditions in considerable detail.

2.2 Linear Stability Theory

Linear perturbation theory has been found to be exceptionally useful as a means for revealing the basic causes of plasma instability in molecular discharges. Detailed discussions of this method as applied to laser discharges are presented elsewhere.[1-4] Certain features of the analysis which are unique to the present treatment of CO laser discharges are briefly discussed in the following paragraphs.

2.2.1 Fractional Derivatives of Rate Coefficients

It has been shown that the sensitivity of plasma processes to small changes in properties such as electron temperature and gas temperature can exert a profound influence on plasma stability, especially in externally sustained discharges.[1] The nature and sensitivity of such variations is conveniently expressed in terms of the fractional, or logarithmic, derivative of electron rate coefficients with respect to electron temperature, i.e.,

$$\hat{k} \equiv \left(\frac{T_e}{k}\right) \frac{\partial k}{\partial T_e} = \frac{\partial \ell n k}{\partial \ell n T_e} \quad . \tag{11}$$

Thus, $\hat{k}$ (or $\hat{\nu}$) is a number, the magnitude and sign of which reveal the nature of the response of a process to a small local change in electron temperature.

In the present analysis k_{VT} exhibits a dependence on n_e, T and n in addition to its dependence on T_e, Eq. (7). It is easily shown that the corresponding fractional derivatives with respect to these variables are simply α, β, and γ, respectively. Similarly, the fractional derivative with respect to gas temperature of the recombination coefficient, k_r^e, is δ.

2.2.2 Electron Temperature Perturbations

In volume-dominated molecular gas discharges, the characteristic time for electron energy relaxation is very short compared to the time required for the charged particle densities to change, so that electron energy kinetics respond to a disturbance in an effectively quasisteady manner on the time scale of importance. On this basis, the first order quasisteady form of the electron energy equation has been used along with Poisson's equation to obtain a relationship coupling disturbances in electron temperature, electron density, and neutral density.[1-4] In the present investigation this procedure has been modified somewhat to account approximately for

the dependence of electron energy loss on vibrational temperature, i.e., the effect of superelastic collisions (Eq. (8)). For conditions such that the electron fractional power transfer to vibration is near unity, the resulting expression relating perturbations in T_e, n_e, n and T_v is,[1-4]

$$\frac{T_{e_k}}{T_e} \simeq \left(\frac{-2\cos^2\phi}{1+\hat{\nu}_u-\hat{\nu}_m\cos 2\phi}\right)\frac{n_{e_k}}{n_e} - \left(\frac{2\sin^2\phi}{1+\hat{\nu}_u-\hat{\nu}_m\cos 2\phi}\right)\frac{n_k}{n}$$

$$+\left(\frac{\zeta\,(T_v/10^4)^{\zeta}\left(1-(T_v/10^4)^{\zeta}\right)^{-1}}{1+\hat{\nu}_u-\hat{\nu}_m\cos 2\phi}\right)\frac{T_{v_k}}{T_v} \qquad (12)$$

$$\equiv \left(\frac{-2\cos^2\phi}{\hat{\nu}_u'}\right)\frac{n_{e_k}}{n_e}+\left(\frac{-2\sin^2\phi}{\hat{\nu}_u'}\right)\frac{n_k}{n}+\left(\frac{\zeta}{\hat{\nu}_u'}\right)\frac{(T_v/10^4)^{\zeta}}{\left(1-(T_v/10^4)^{\zeta}\right)}\frac{T_{v_k}}{T_v},$$

where T_{e_k}, n_{e_k}, n_{n_k}, and T_{v_k} are the amplitudes of the k'th Fourier components of the respective perturbed properties,[1-4] and where ν_u and ν_m are the total electron energy exchange and momentum transfer collision frequencies, respectively, the caret notation referring to logarithmic derivatives of these collision frequencies with respect to electron temperature as described previously. In this equation the angle ϕ is the angle between the direction of the zeroth order (anticipated steady-state) electric field and the wave propagation vector $\underset{\sim}{k}$.[1-4]

2.2.3 First Order Stability Equation

With the considerations discussed above providing the basis for the approach to be followed, linear stability analysis is applied to Eqs. (1)-(5) as described previously.[1-4] This procedure results in the following system of first order equations relating the perturbation amplitudes n_{e_k}, n_{n_k}, T_k, T_{v_k}, and T_{e_k} and the anticipated steady state properties:

$$\left(\frac{n_{e_k}}{n_e}+\frac{T_k}{T}\right)\nu_k = -\frac{n_{e_k}}{n_e}\left[\frac{n_n}{n_e}\,nk_d+\frac{n_e}{n_p}\,n_p k_r^e+\frac{n}{n_e}\,S_E\right]$$

$$+\frac{n_{n_k}}{n_n}\left[\frac{n_n}{n_e}\,nk_d-\frac{n_n}{n_p}\,n_p k_r^e\right]-\frac{T_k}{T}\left[n_p k_r^e-\frac{n_n}{n_e}\,nk_d\hat{k}_d-n^2k_{a_2}+\delta n_p k_r^e\right] \qquad (13)$$

$$+\frac{T_{e_k}}{T_e}\left[nk_i\hat{k}_i-n_p k_r^e\hat{k}_r^e-nk_{a_1}\hat{k}_{a_1}-n^2k_{a_2}\hat{k}_{a_2}\right],$$

$$\left(\frac{n_{n_k}}{n_n} + \frac{T_k}{T}\right)\nu_k = \frac{n_{e_k}}{n_e}\left[\frac{n_e}{n_n}(nk_{a_1} + n^2 k_{a_2}) - \frac{n_e}{n_p} n_p k_r^i\right]$$

$$- \frac{n_{n_k}}{n_n}\left[\frac{n_n}{n_p} n_p k_r^i + \frac{n_e}{n_n}(nk_{a_1} + n^2 k_{a_2})\right] + \frac{T_{e_k}}{T_e}\left[\frac{n_e}{n_n}(nk_{a_1}\hat{k}_{a_1} + n^2 k_{a_2}\hat{k}_{a_2})\right] \qquad (14)$$

$$- \frac{T_k}{T}\left[n_p k_r^i (1 + \hat{k}_r^i) + nk_d \hat{k}_d + \frac{n_e}{n_n} n^2 k_{a_2}\right] \quad ,$$

$$\frac{T_k}{T}\nu_k = \frac{T_k}{T}\left[-\frac{\kappa k^2}{nC_p} - \frac{JE}{nC_pT}\left[F_v\left(1-(T_v/10^4)\zeta\right)(2-\beta+\gamma) + F_T\right]\right]$$

$$+ \frac{T_{v_k}}{T_v}\left[\frac{F_v JE}{nC_pT}\left(1-(T_v/10^4)\zeta\right)\right] + \frac{JE}{nC_pT}\left[\frac{n_{e_k}}{n_e}\left(F_T + F_v\,\alpha\left(1-(T_v/10^4)\zeta\right)\right)\right. \qquad (15)$$

$$\left. + \frac{T_{e_k}}{T_e}\left(F_T(1+\hat{\nu}_T) + F_v \hat{k}_{VT}\left(1-(T_v/10^4)\zeta\right)\right)\right] \quad ,$$

$$\frac{T_{v_k}}{T_v}\nu_k = \frac{T_k}{T}\left[\frac{JE}{X_m nkT_v}\left[F_v\left(1-(T_v/10^4)\zeta\right)(2-\beta+\gamma) - F_v\right]\right.$$

$$- \frac{T_{v_k}}{T_v}\left[\frac{F_v JE}{X_m nkT_v}\left(1-(T_v/10^4)\zeta\right)\left[1 + \frac{\zeta(T_v/10^4)^\zeta}{\left(1-(T_v/10^4)^\zeta\right)}\right]\right] \qquad (16)$$

$$\left. + \frac{F_v JE}{X_m nkT_v}\left(1-(T_v/10^4)\zeta\right)\left[\frac{n_{e_k}}{n_e}(1-\alpha) + \frac{T_{e_k}}{T_e}(1+\hat{\nu}_v - \hat{k}_{VT})\right]\right] \quad ,$$

where ν_k is the growth or damping rate of coupled disturbances in n_e, n_n, T, T_v, and T_e. In the derivation of these equations it has been assumed that first order pressure fluctuations are very small, a condition permitting replacement of n_k/n by $-T_k/T$. This approximation is valid as long as the characteristic time for the dissipation of acoustic disturbances is much less than the time required for evolution of disturbances in thermal and vibrational energy density, a condition usually satisfied in cw or quasi-cw convection discharges.

SECTION 3

THERMAL INSTABILITY

3.1 Basic Considerations

3.1.1 Steady State Properties

Numerical experimentation carried out previously[1] has shown that once the ranges of steady state plasma properties such as pressure, gas mixture, electron temperature, electron density, and electrical power density have been established, thermal instability is far more sensitive to specific microscopic details of electron production and loss processes than to variations in the values of macroscopic plasma conditions. Thus, by establishing reasonable values for the steady state properties the influence on thermal instability of changes in those processes affecting electron production and loss and vibrational relaxation can be examined in detail.

In this investigation conditions were selected so as to be representative of an externally sustained CO laser plasma in a supersonic flow. Conditions at the discharge inlet were taken as P_o = 100 Torr, T_o = 65°K, U_o = 10^5 cm/sec, with CO and He in the proportions 0.1 - 0.9. The external ionization source, S_E, was assumed to be uniform throughout the volume. For these conditions the flow is supersonic with the gas density and flow velocity essentially independent of position in the discharge region. Figure 4 presents computed spatial variations of T and T_v for representative conditions. In this example electrons were assumed to be lost by recombination depending only on T_e, with the result that the electron density and electron temperature are both independent of position.

The required electron collision frequency data for the CO-He 0.1:0.9 mixture considered in this analysis were computed and are presented in Fig. 5, while the corresponding fractional derivatives for this mixture are shown in Fig. 6. The factors influencing the magnitude and electron temperature dependence of these data are well understood and are found to be generally similar for a variety of mixtures of importance in CO laser applications. It is worth pointing out however, that $\hat{\nu}_u$ and $\hat{\nu}_v$ exhibit very large variations in the region of electron temperature for which vibrational excitation is most efficient.

3.1.2 Electron Ion Recombination Data

Processes involving CO itself should lead to no net negative ion production in CO laser discharges.[2,3] Further, in this analysis it is assumed that the impurity $Fe(CO)_5$, which is invariably present in CO[10-12], can be reduced to a level such that electron dissociative attachment involving $Fe(CO)_5$ is unimportant, i.e., < 10 ppm.

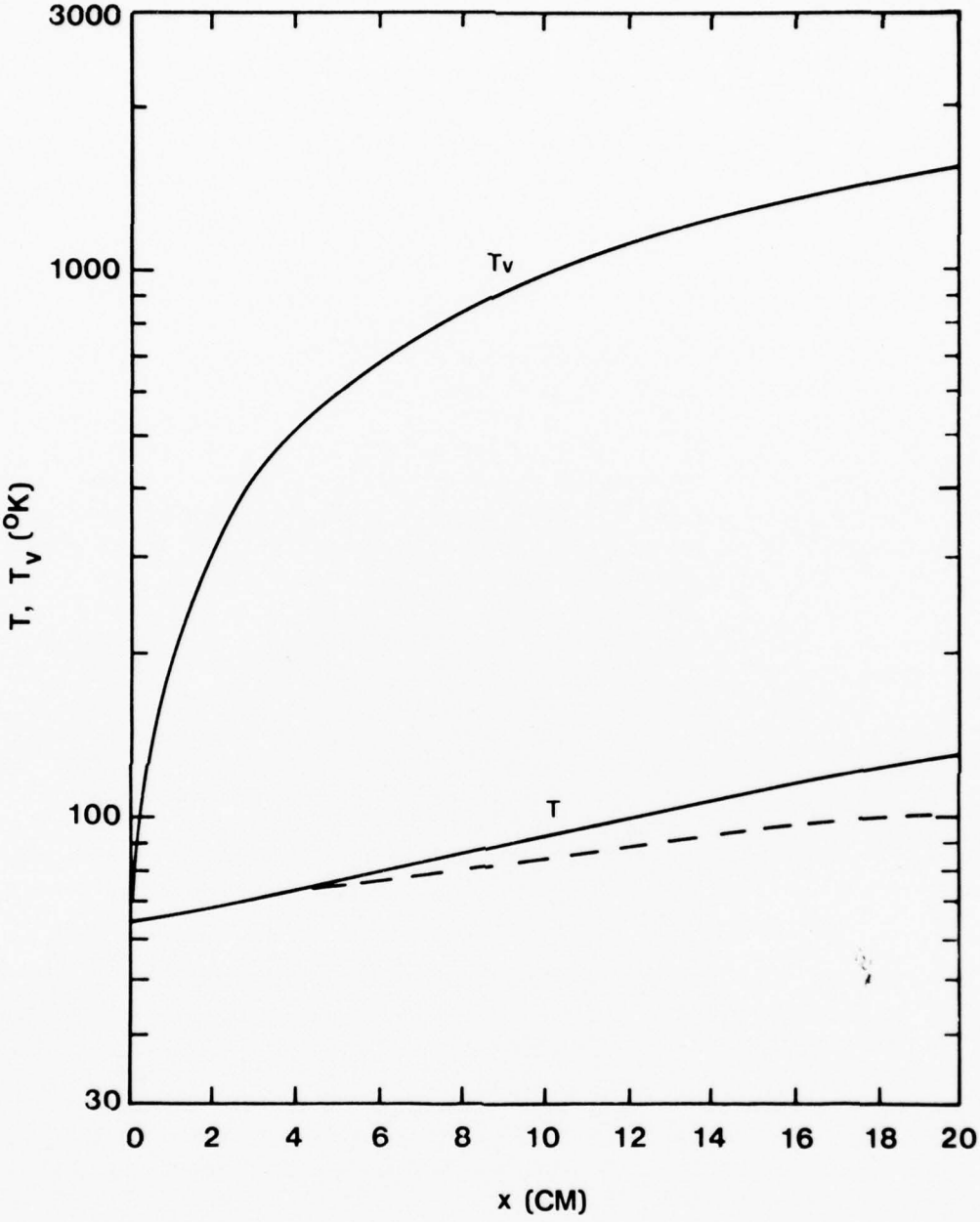

Figure 4. Computed spatial evolution of T_v and T from the discharge entrance for the base mixture and initial pressure of Figs. 1-3 and the following conditions: $E/n = 0.88 \times 10^{-17}$ V cm^2, $U_o = 10^5$ cm/sec and $S_E = 3.4 \times 10^{-3}$ cm^{-1}. The dashed curve shows the temperature variation assuming 50% of the power transferred to vibration is extracted as laser power; in the presentation of all subsequent data such will be assumed to be the case.

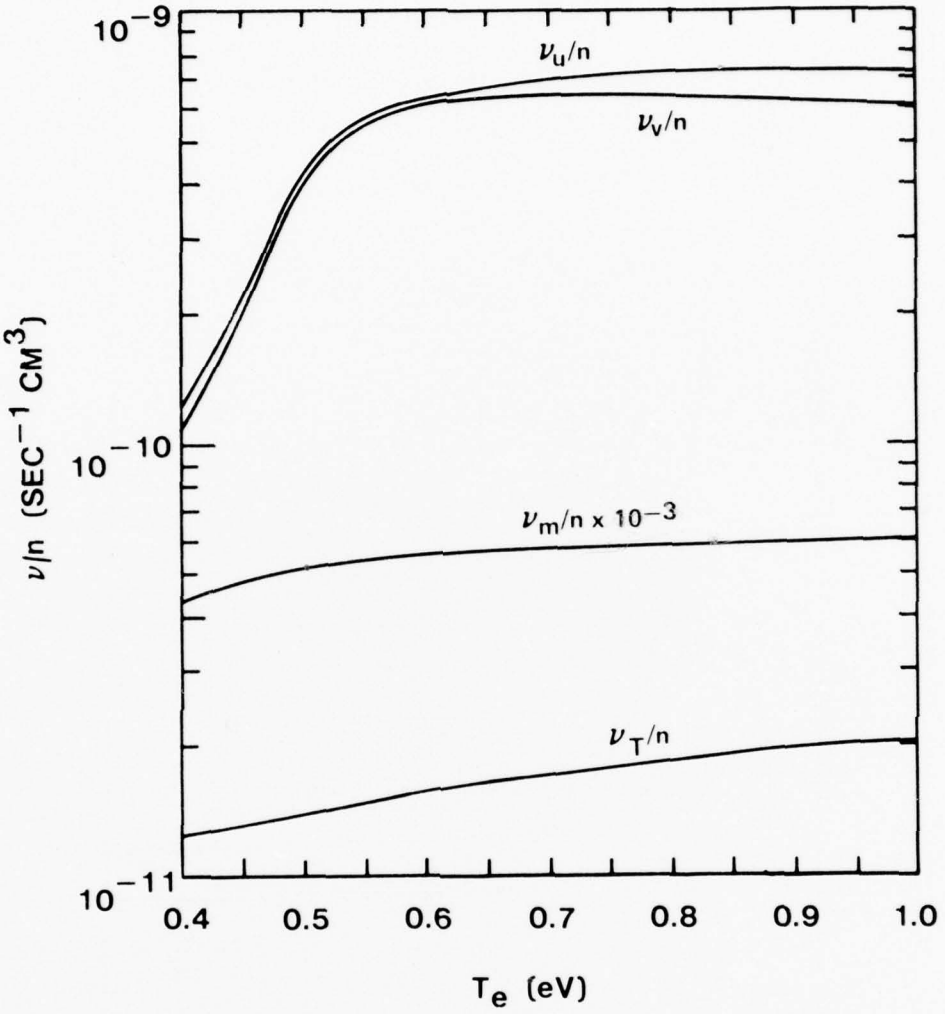

Figure 5. Electron-molecule collision frequencies for total energy transfer, ν_u, vibrational excitation, ν_v, translational-rotational heating, ν_T, and momentum transfer, ν_m, computed for a CO-He (0.1:0.9) mixture.

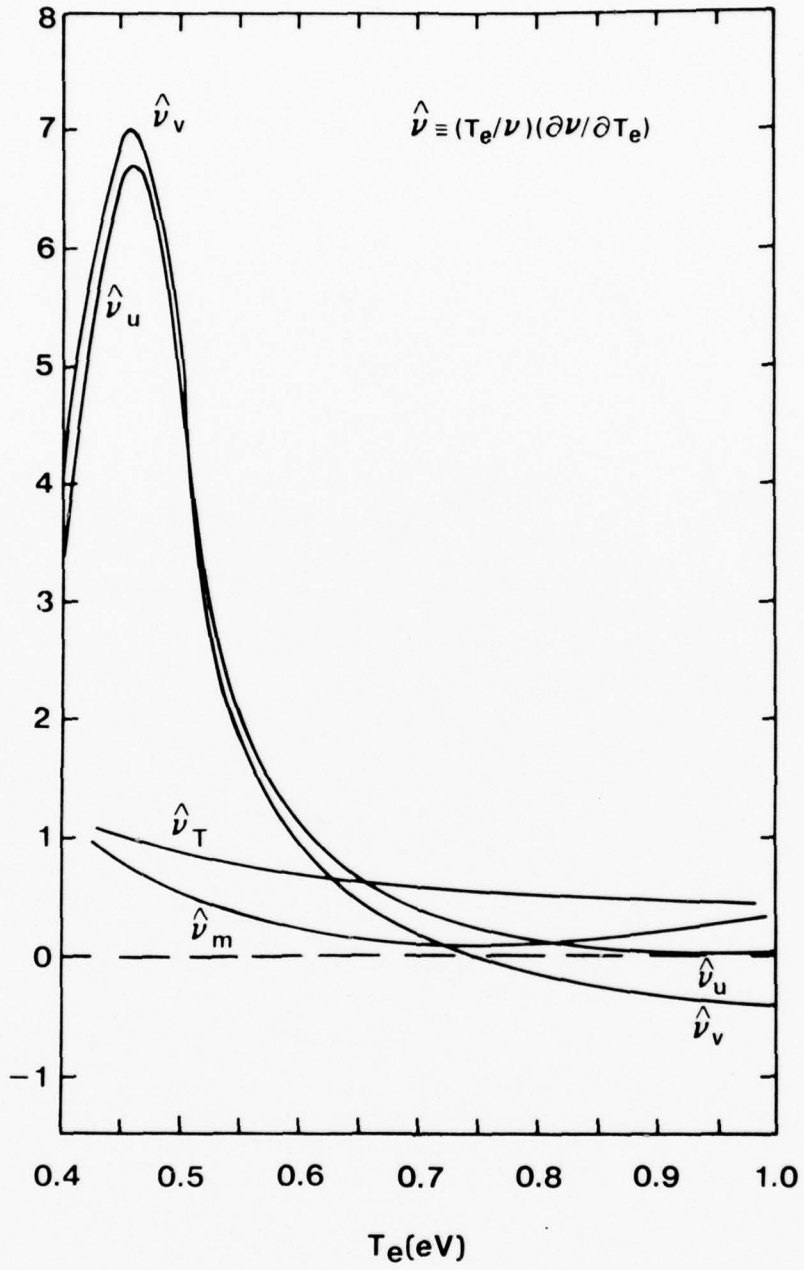

Figure 6. Fractional derivatives of the electron collision frequency data presented in Fig. 5. Values of $|\hat{\nu}| < 1$ imply a relatively weak dependence on electron temperature.

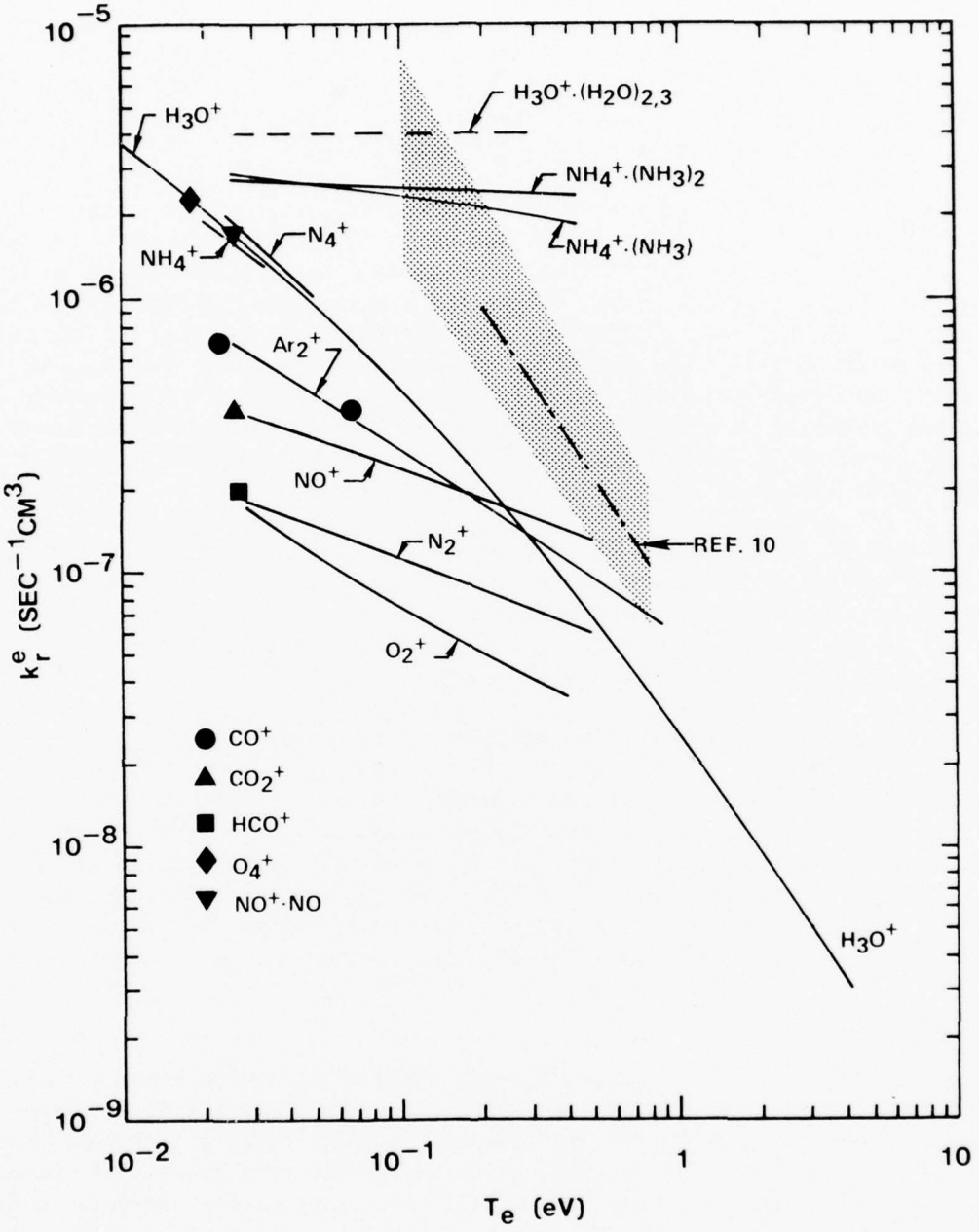

Figure 7. Summary of electron-ion recombination coefficient data. These data and their sources are discussed in Ref. 9. The data for H_3O^+ are from R. A. Heppner, F. L. Walls, W. T. Armstrong and G. H. Dunn (Phys. Rev. A13 1000 (1976)). The data of Refs. 10, 13, and 14 in which the ion species were not identified fall within the shaded region.

With this proviso, the negative ion concentration should be relatively low in CO laser plasmas ($n_n/n_e \ll 1$), with electron loss dominated by recombination. Figure 7 provides a summary of nearly all the molecular recombination coefficient data available as a function of electron temperature (Maxwellian energy distribution). These data along with their sources, are discussed in Ref. 9.

Recently, measurements of electron recombination under ambient pressure and temperature conditions have been carried out using N_2[13], CO[10], and CO_2 laser mixtures.[14] These data were obtained under conditions generally similar to externally sustained laser discharges, and fall within the shaded region of Fig. 7. In the N_2 and CO measurements the positive ions were assumed to be N_4^+ and $CO^+.CO$, respectively, or perhaps higher order polymers. In these measurements the electron energy distribution was not Maxwellian. Thus, in Refs. 10, 13, and 14 recombination coefficients are presented as a function of mean or characteristic electron energy, a circumstance that could introduce as much as a factor of 2 variation in the inferred k_r^e value even for the same ion.

Of particular importance to this study are the data of Ref. 10 for CO which are specifically indicated in the shaded region of Fig. 7. The inferred recombination coefficient in CO exhibits a $T_e^{-3/2}$ variation (i.e., $\hat{k}_r^e = -1.5$) and will be used as a reference in the stability computations to be discussed in subsequent sections.

3.2 Thermal Instability Growth Rates

Following the procedure described in detail in Ref. 1, Eqs. (13)-(16) were numerically solved in terms of the anticipated properties in the discharge region. For all conditions examined the plasma was found to be thermally unstable ($\nu > 0$), having a growth rate strongly peaked in the direction normal to the electric field ($\varphi = 90^o$). This behavior is indicative of vibrational/thermal instability driven by disturbances in electron-molecule vibrational excitation.[1]

3.2.1 Growth Rates

Presented in Fig. 8 are computed thermal instability growth rates as a function of E/n corresponding to the plasma conditions discussed in preceding sections. These calculations (curve a) show that as the electrical power density increases in the 100-1000 W/cm^{-3} range the time characterizing the growth of thermal disturbances (ν^{-1}) decreases from approximately 10^{-3} to 10^{-4} sec. The rather sharp increase in the growth rate in the 500-700 W/cm^3 range reflects the onset of ionization due to low energy electron impact. As pointed out previously,[1] avalanche ionization become significant as regards thermal instability growth when the steady state contribution of low energy electron-molecule ionization is only about 1 percent of that due to the external source (this point is indicated by the arrow in the figure).

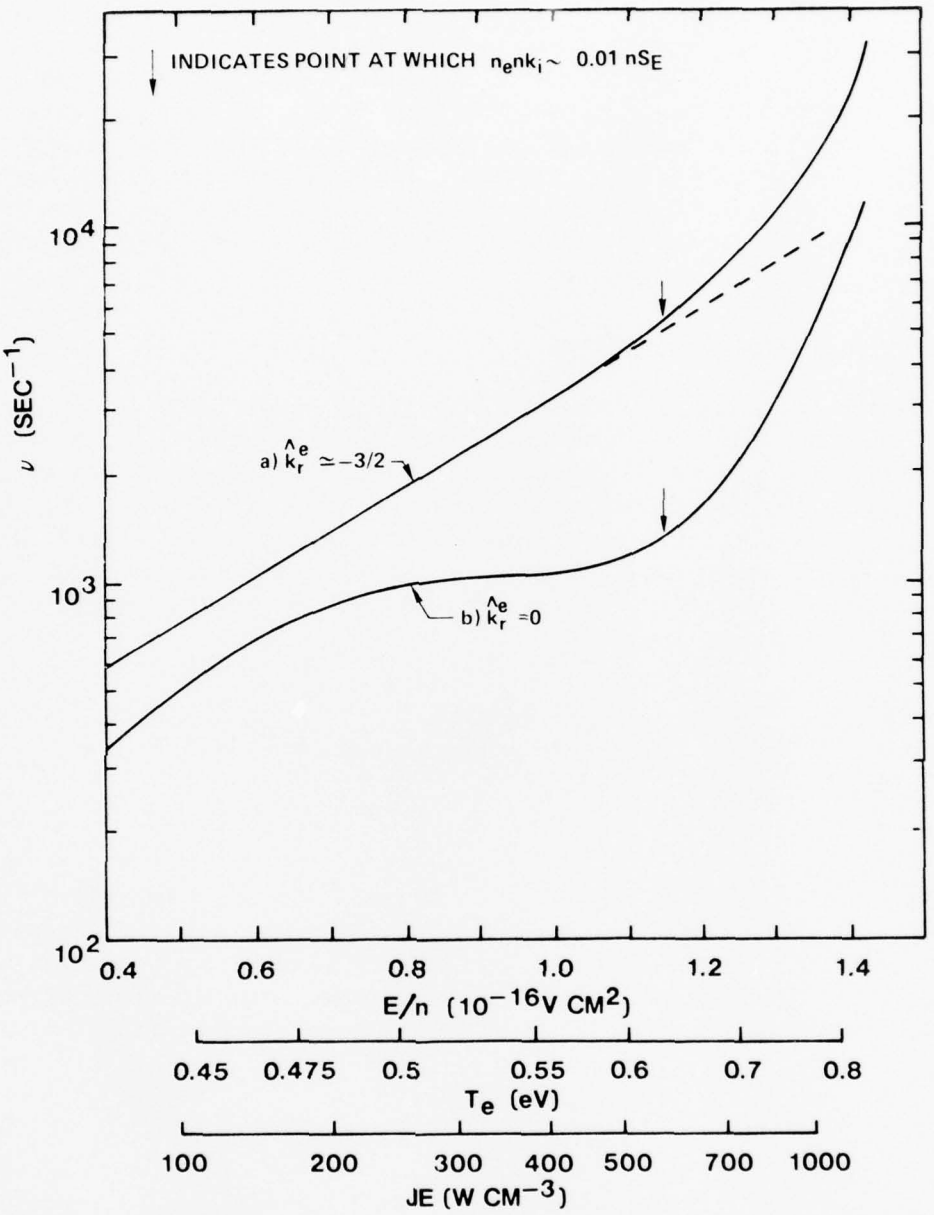

Figure 8. Computed thermal instability growth rate in the direction normal to the electric field ($\varphi = 90^{\circ}$) for the base conditions of Figs. 1-4 and a source function, S_E, of 3.4×10^{-3} sec^{-1}. Curve a was generated using the k_r^e data of Ref. 10 obtained in CO under atmospheric density conditions; the growth rate computed on this basis will be the reference for all subsequent comparisons. Curve b was generated using a constant k_r^e value of 2.0×10^{-7} sec^{-1} cm^3.

For the purpose of comparison Fig. 8 also shows the growth rate computed using a constant value of 2×10^{-7} sec^{-1} cm^3 for the electron recombination coefficient, i.e., $\hat{k}_r^e = 0$. Clearly, the effect on the growth rate is very significant resulting in a factor of 2 to 3 decrease in ν over the range of variables considered. Numerical experimentation with the exponents α, β and γ (Eq. (7)), which reflect the sensitivity of V-T relaxation to changes in n_e, T and n was found to have a far smaller effect on the growth rate. In fact, taking k_{VT} as a constant having a magnitude consistent with the reference conditions indicated in Fig. 2 was found to have a small effect compared to reasonable variations in the electron recombination coefficient.

3.2.2 Electron Density Disturbances

For reasons discussed in detail in Ref. 1, the sensitivity of the growth rate exhibited by the data of Fig. 8 to seemingly minor changes in the nature of the electron loss process is readily understood by examination of the change in the electron density disturbance. Figure 9 shows the computed variation of the fractional electron density disturbance relative to a change in gas temperature, i.e., $(n_{e_k}/n_e)(T_k/T)^{-1}$, corresponding to curves a and b in Fig. 8. To a first approximation the instability growth rate is related to the fractional electron density disturbance by the expression,[1]

$$\nu_k \sim \frac{JE}{nc_pT}\left(1 + \frac{n_{e_k}/n_e}{T_k/T}\right) \; ; \; \phi \sim 90^\circ \; . \tag{17}$$

Although the magnitude of $(n_{e_k}/n_e)(T_k/T)^{-1}$ is small (in fact, negative) compared to its value in a self-sustained plasma (> 10), the increase in the electron density disturbance caused by a recombination loss which decreases with electron temperature is very significant. When avalanche ionization approaches 1 percent of that due to the external source $(n_{e_k}/n_e)(T_k/T)^{-1}$ begins to increase very rapidly as is indicated in Fig. 9.

3.2.3 O_2 Molecular Ions

There exists considerable evidence that small quantities ($\lesssim 1$ percent) of O_2 added to CO laser discharges enhances their stability.[15,16] Theoretical[17] and experimental[16] investigation of the role of O_2 in low pressure (10 Torr) diffusion cooled CO laser discharges indicates that when O_2 is present the initial clustered positive ion species charge exchanges with O_2 resulting in the simple molecular ion O_2^+. The extension of these findings to high pressure[15] CO discharges is open to question for reasons to be discussed in Sec. 4. Nonetheless, instability growth rates were computed for comparison with the data in Fig. 8 by assuming that

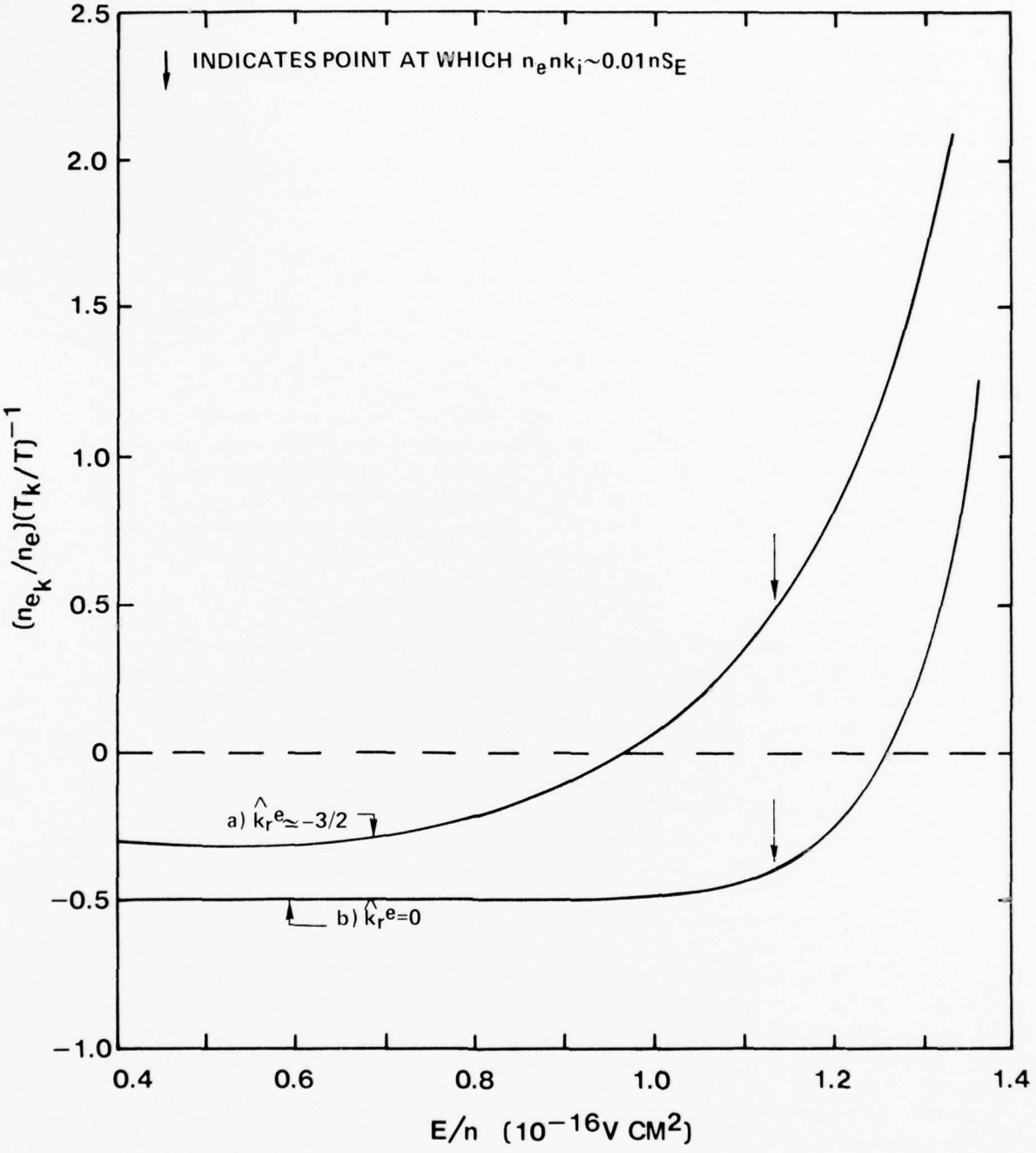

Figure 9. Fractional electron density disturbance relative to a disturbance in gas temperature corresponding to the data of Fig. 8.

approximately 1 percent O_2 added to the CO-He (0.1:0.9) mixture resulted in conversion of all positive ions to O^+_2. The electron recombination coefficient shown in Fig. 7 for O_2^+ was used in the calculations. Because k_r^e for O_2^+ is substantially lower in magnitude than the recombination coefficient used here as a reference (from Ref. 10), the magnitude of the external source function was reduced so as to yield the same electron density (and power density) at an electron temperature of about 0.4 eV.

The results of this calculation are presented in Fig. 10. For the lower values of E/n $\nu(O_2^+)$ is very similar to curve b in Fig. 8, even though the magnitude of $k_r^e(O_2^+)$ is 5 to 10 times smaller than the 2 x 10^{-7} $sec^{-1}cm^3$ value used in the generation of curve b, Fig. 8. This reflects the fact that as long as the characteristic time for recombination is short compared to the instability growth time ($n_e k_r^e \gg \nu$) the electron density response will be quasisteady.[1] When this is the case only the electron temperature dependence of the recombination coefficient as reflected by the magnitude and sign of $\hat{k}_r^e$ affects thermal instability growth; the magnitude of k_r^e itself has little or no effect. As E/n increases the data of Fig. 10 show that the onset of avalanche ionization occurs at a lower T_e value when k_r^e for O_2^+ is used. This is to be expected since the electron production required by the external source is reduced as a consequence of the lower $k_r^e(O_2^+)$ value.

In Fig. 11 the computed growth rates of Fig. 10 are presented as a function of electric power density. Presentation of the data in this form shows that while the premature onset of avalanche ionization occurs at lower E/n levels when O_2^+ is assumed to be the dominant ion, the instability growth rate tends to saturate at higher power density levels unlike the growth rate obtained using the reference k_r^e value. This behavior is a finite kinetics effect reflecting the inability of the electron density to respond to neutral particle disturbances in a quasisteady manner, i.e., $n_e k_r^e(O_2) \not\gg \nu$. When this occurs both the magnitude and the electron temperature dependence of the recombination coefficient affect the instability growth rate.

When thermal instability growth rates were computed for the self-sustained discharge conditions typical of Ref. 15 in which O_2 addition was found to improve plasma stability, the finite temporal response of the electron density was found to be significant. Indeed, the instability growth rate corresponding to a specific power density was reduced by approximately 50 percent when k_r^e for O_2^+ was used in the calculations. The computed instability growth times (ν^{-1}) were also found to be nearly equivalent to plasma residence time in the discharge.[1,2] However, it must be pointed out that there is little reason to expect O_2^+ to be the dominant ion at the high pressures used in Ref. 15.

3.2.4 Gas Temperature Dependent Recombination

For the reasons given in Sec. 2 and elaborated upon in Sec. 4 the positive ion species typical of CO and CO_2 high power discharge conditions will be clusters. Many clustered ions have weak bond energies with the result that cluster ion equilibrium, and therefore recombination, is exceptionally sensitive to variations in gas

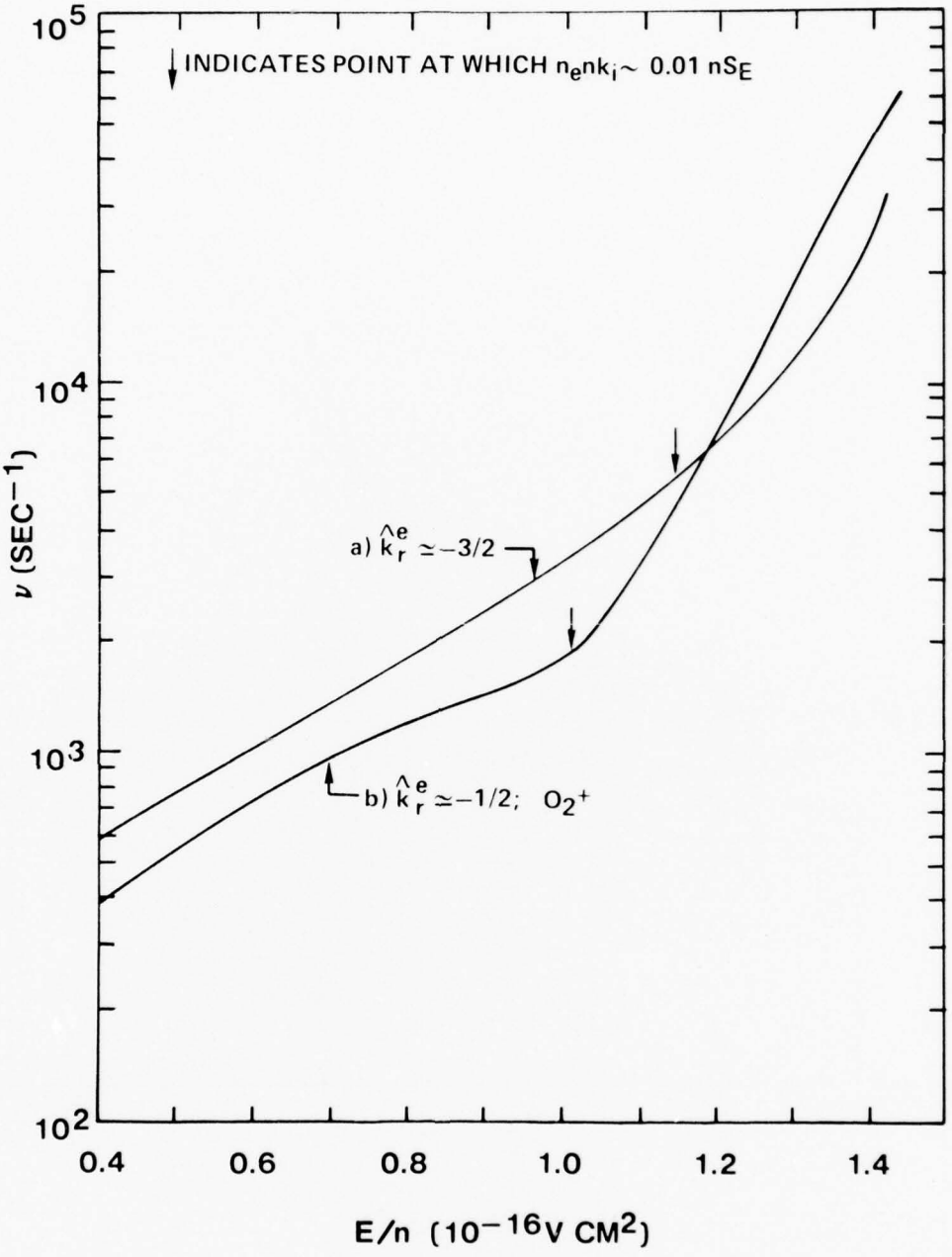

Figure 10. Thermal instability growth rate using the reference k_r^e data of Ref. 10, curve a, compared with the growth rate assuming O_2^+ is the dominant ion, curve b.

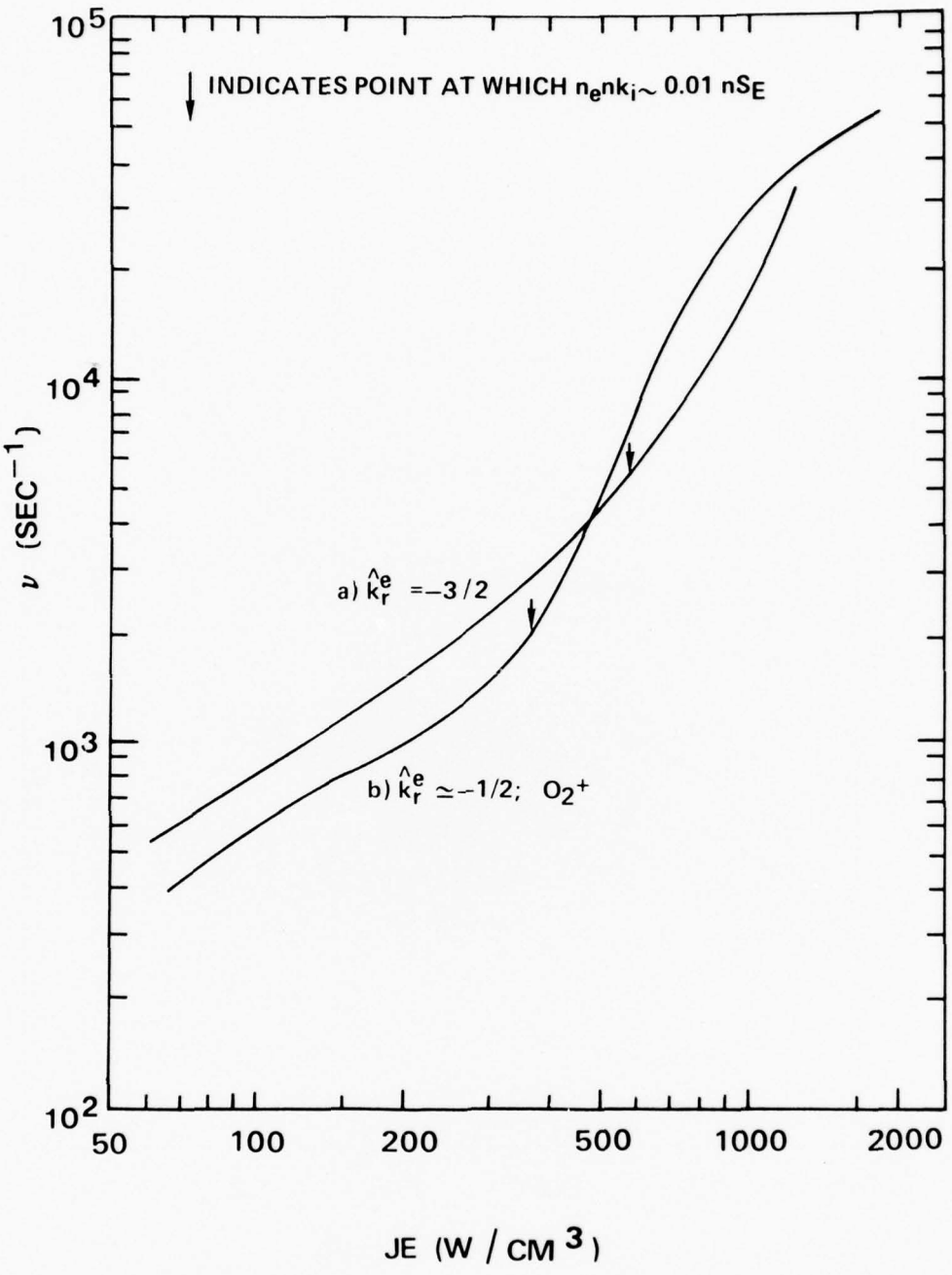

Figure 11. Instability growth rate data of Fig. 10 presented as a function of electrical power density.

temperature. In order to evaluate the effect of a gas temperature dependent recombination loss, instability growth rates were computed for various values of the exponent δ in Eq. (10). The results of these calculations are presented in Fig. 12. As anticipated, the effect on the instability growth rate is profound with ν increasing by about an order of magnitude as δ is varied from 0 (base case) to -10.

To the same level of approximation used in deriving Eq. (17) it can be shown that the fractional electron density disturbance is related to δ by the equation,

$$\frac{n_{e_k}/n_e}{T_k/T} \simeq -\frac{1}{2}\left[1+\delta+\frac{2\hat{k}_r^e}{\hat{\nu}_u'}\right] \quad ; \quad \phi \sim 90^\circ \quad . \tag{18}$$

Thus, as δ becomes increasingly negative the recombination loss decreases more during a disturbance resulting in an increase in the electron density disturbance. Figure 13 presents the computed values of $(n_{e_k}/n_e)(T_k/T)^{-1}$ as a function of δ corresponding to the conditions of Fig. 12 at an E/n value of 1.0×10^{-16} Vcm^2 ($T_e \sim 0.55$ eV). The increase in the electron density disturbance is dramatic indeed. These results and those discussed in Sec. 4 vividly illustrate the importance of obtaining significantly better information on ion loss processes in high pressure laser discharges.

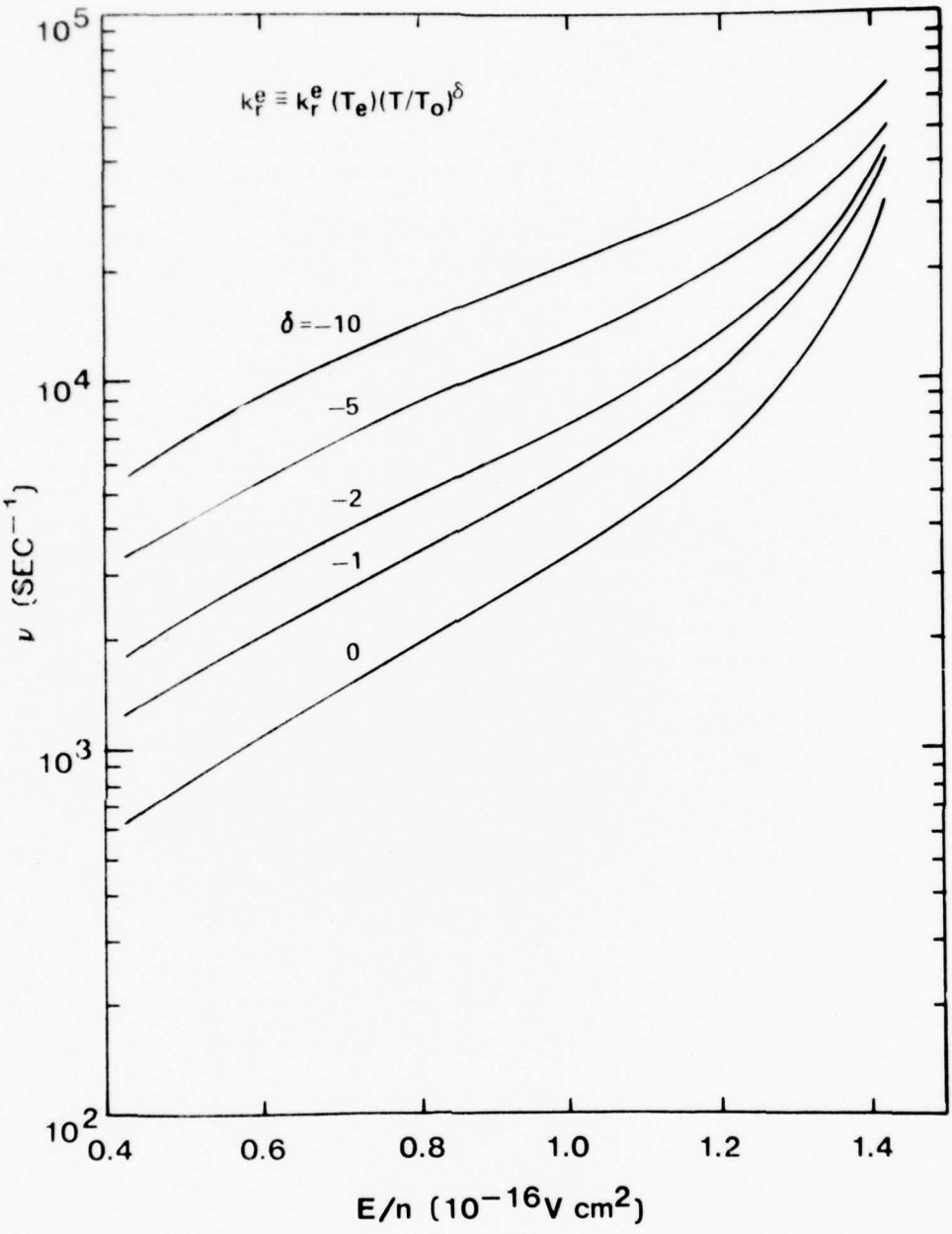

Figure 12. Dependence of the thermal instability growth rate for the reference conditions on a gas temperature dependent recombination coefficient (See Eq. (10) and Sec. 3.2.4).

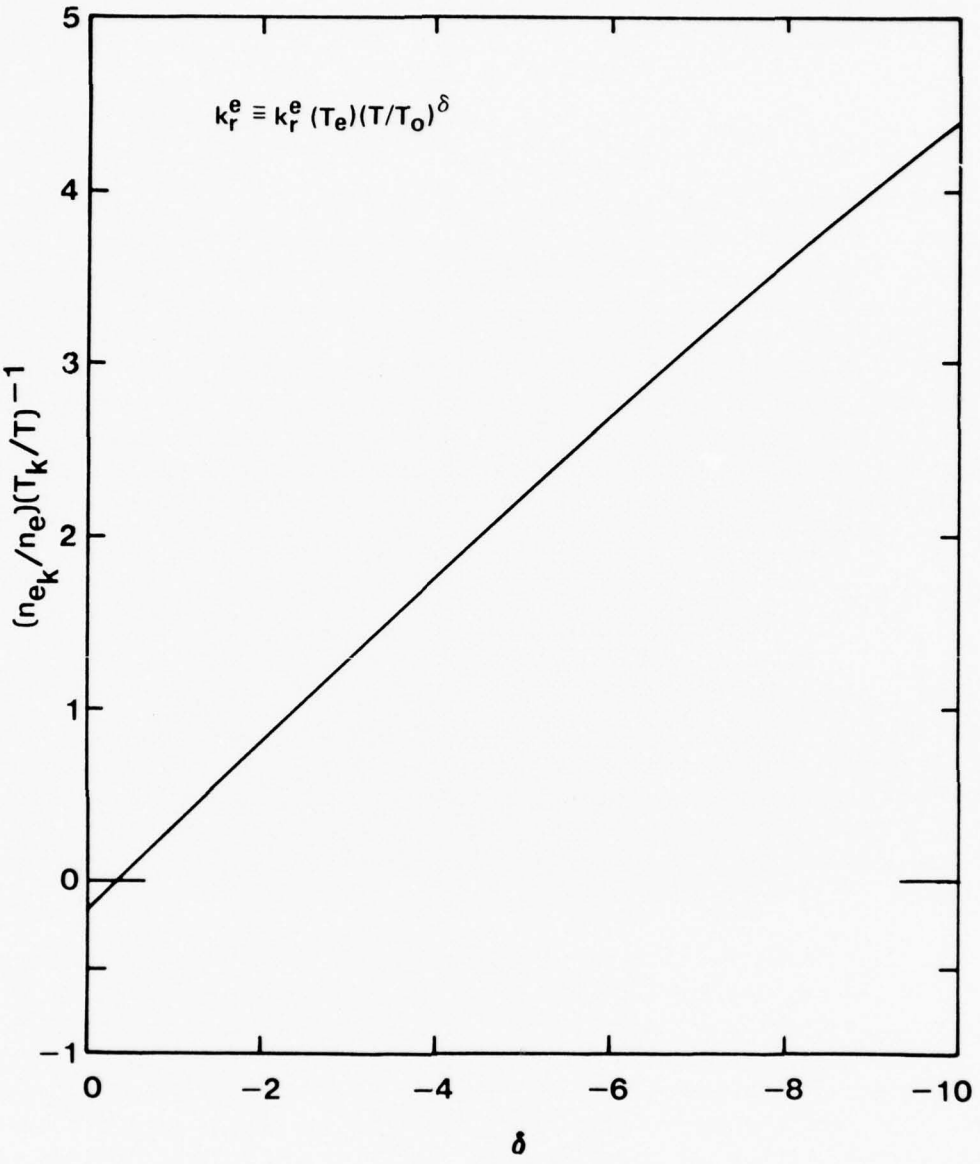

Figure 13. Fractional electron density disturbance corresponding to the data of Fig. 12 for an E/n value of 0.88×10^{-16} V cm^2 ($T_e \simeq 0.52$ eV).

SECTION 4

POSITIVE ION CHEMISTRY

The very low fractional ionization ($n_e/n \simeq n_p/n \sim 10^{-8} - 10^{-7}$) characterizing both CO and CO_2 electric discharge lasers is a unique feature which may impact significantly on plasma stability. It is well known that even with scrupulous cleanup and drying it is very difficult to reduce the water molecule concentration in atmospheric gases to below 10 ppm.[18-20] Even the concentration of $Fe(CO)_5$ in CO cannot be reduced below about 1 ppm.[10] Therefore it is clear that the concentration of residual impurities such as H_2O in molecular laser mixtures will always exceed the electron concentration by at least a factor of ten. Because of the likely impurity level and fast ion conversion kinetics it is probable that the dominant positive ion species in laser mixtures will not be related to the constituents of the parent gas.

4.1 Hydrated-Hydronium Ion Sequence

In high power laser applications the ions produced initially by the external source are related to the major constituents of the gas. However, as a consequence of charge exchange, rearrangement and switching reactions[21-24] the terminal ions are frequently found to be $H_3O^+ \cdot (H_2O)_n$, with the detailed distribution depending on temperature and water concentration.[18-20] The equilibrium constants for the hydrated-hydronium ion sequence have been measured[25] from which the various members of the sequence are easily determined.

Figure 14 presents the fractional concentration of hydrated-hydronium ions as a function of temperature and H_2O pressure. These data were computed on the basis of the information presented in Ref. 25. Under ambient atmospheric conditions with 1 to 10 ppm H_2O present the ion sequence will be dominated by relatively large n values, e.g., $n > 3$. Moreover, experiments[24] in N_2 at a pressure of only 10^{-3} atm have shown that equilibrium is established for this ion series in a few hundred μsec. Since most of the ion rearrangement reactions are three-body involving the background gas, it is clear that at the atmospheric densities typical of high power CO and CO_2 lasers ion equilibrium will be achieved on a μsec time scale.

Recent ion identification measurements have been found to be in good agreement with predictions based on the available equilibrium constants. Figure 15 shows a positive ion mass spectrum[20] obtained in exceptionally clean air having an H_2O concentration of approximately 3 ppm. Essentially the same ion spectrum was obtained in "pure" N_2. In all cases the $H^+ \cdot (H_2O)_n$ series was found to be dominant. Comparison of Figs. 14 and 15 shows very good agreement between the predicted and measured ion spectrum.

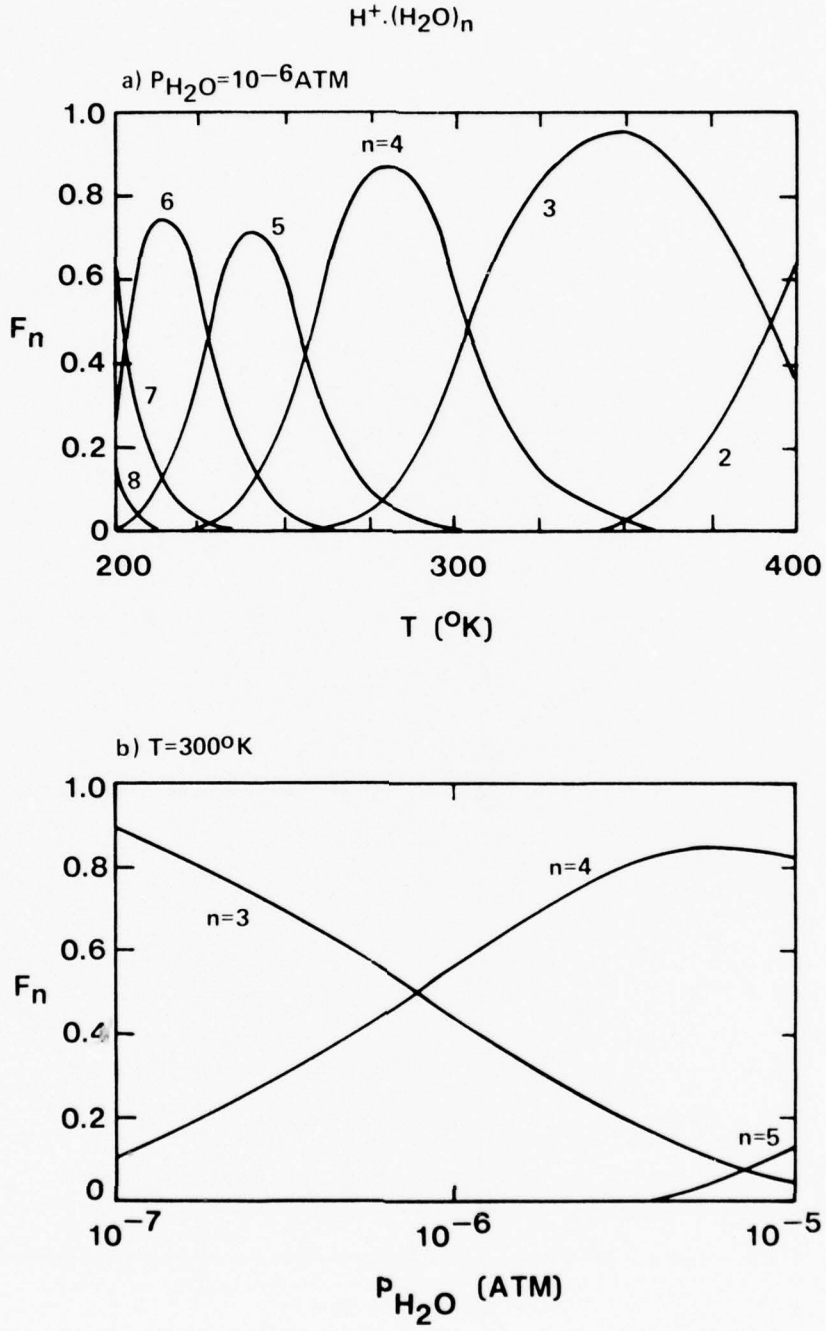

Figure 14. Fractional concentration of $H^+\cdot(H_2O)_n$ series ions computed using the equilibrium constants of Ref. 25.

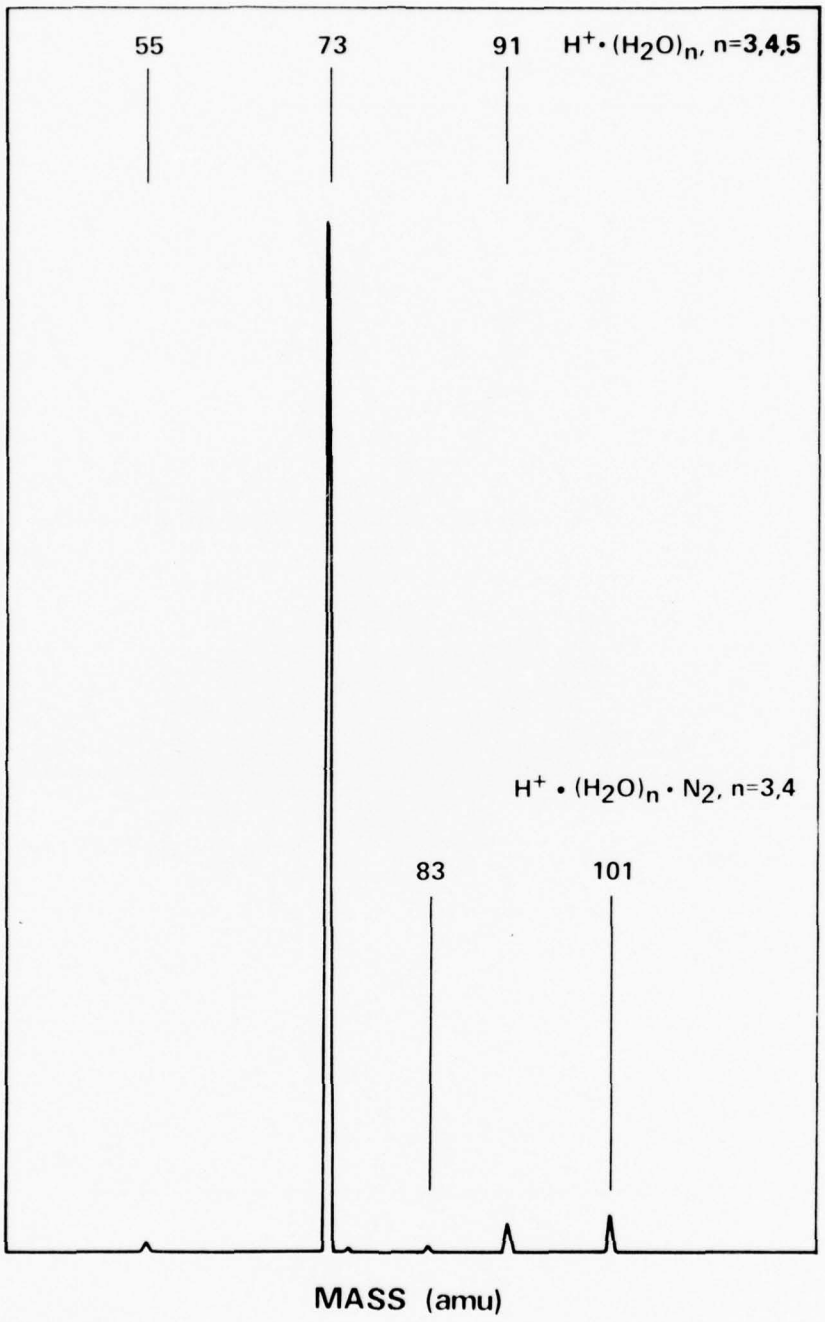

Figure 15. Measured positive ion spectrum in clean, very dry (~3 ppm H_2O) air at atmospheric density and ambient temperature. (From Kadlecek, Ref. 20).

For purposes of comparison, Fig. 16 shows measured[26] values of fractional ion concentration as a function of E/n in a CO_2-N_2-He (1:2:3) laser mixture at 0.38 Torr containing H_2O at 10^{-3} Torr ($\sim 10^{-6}$ atm). Even at this low pressure the hydrated-hydronium series ion was found to dominate. Agreement with the analytical data of Fig. 14 is very good at low E/n values at which $T_{ion} = T$. Measurements[7] of ion identity in CO have also been made at very low pressures (.01-0.35 Torr) and at relatively low residual H_2O levels (10^{-5}-10^{-4} Torr, $< 10^{-7}$ atm). Even under these conditions the dominant ion species at room temperature and a CO pressure of 0.35 Torr were found to be $CO^+ \cdot H_2O$ and H_3O^+. The cluster $CO^+ \cdot CO$ was found to be the dominant ion only in a narrow range of pressures between 0.1 and 0.3 Torr.

In light of the findings discussed in the preceding paragraphs it appears almost certain that the experimental conditions typical of recent high pressure recombination measurements[10,13,14] are not consistent with the occurrence of simple molecular ion species such as N_4^+, $CO^+ \cdot CO$, or even higher order members of these sequences. While the recombination data falling within the shaded region in Fig. 7 are representative of electron recombination loss under conditions generally similar to those in laser discharges, considerable caution should be exercised when interpreting their meaning. Of course, until the ions are actually identified experimentally for conditions typical of CO laser discharges it is not possible to state flatly that the hydrated-hydronium sequence will be dominant. For example, even in a mixture containing only CO and He (or Ar) as major constituents the ion clusters may be of a more complex form, e.g., $H_3O^+ \cdot (H_2O)_n \cdot (CO)_m$. The presence of other major additives such as N_2, O_2 and H_2 along with the contaminant $Fe(CO)_5$ further complicates matters especially in a discharge environment. For these reasons, while the exact species of ions remain unknown, it can be concluded with some certainty that relatively simple molecular ions typical of the parent gas will not be dominant for CO (or CO_2) electric discharge laser conditions.

4.2 Cluster-Ion Recombination

The preceding conclusions are likely to have a very important bearing on CO and CO_2 laser stability for the following reasons: (1) measured[27] values of the electron recombination coefficient for hydrated-hydronium series ions are one to two orders of magnitude larger than simple molecular ions; (2) the electron temperature dependence of these clustered ions has recently been found to be very weak[28] as indicated in Fig. 7; and (3) the ion cluster bond energies[25] are relatively weak (< 1.0 eV) with the result that the quasisteady cluster ion distribution actually obtained under specific conditions will be exceptionally sensitive to the neutral and ion translation temperatures and almost certainly to the vibrational temperature as well. Indeed, there is every reason to presume the electron temperature dependence of the recombination coefficient inferred from the data of Refs. 10, 13, 14 also relfects variations in the ion translational temperature and neutral vibrational temperature, both of which increase as E/n increases.

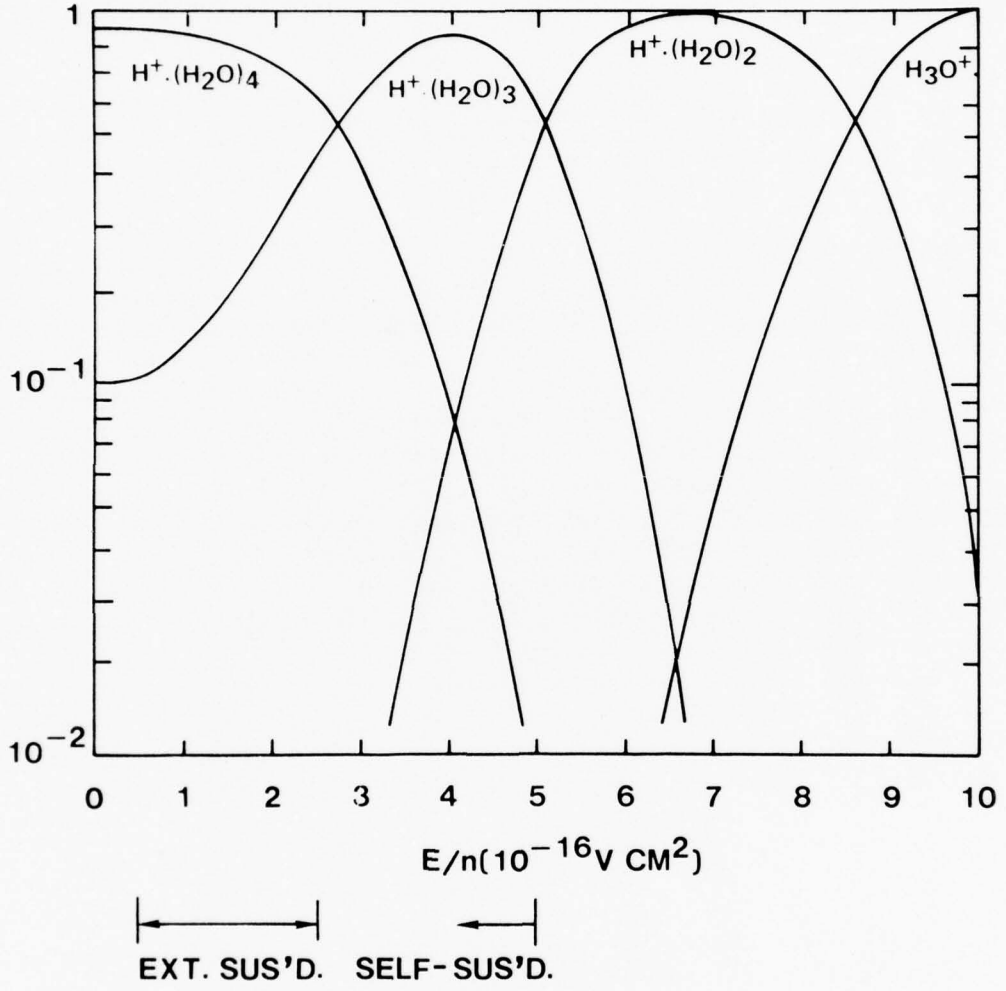

Figure 16. Fractional concentration of $H^+\cdot(H_2O)_n$ series ions in a 0.38 Torr CO_2-N_2-He laser mixture at 300°K (From McFarland, Albritton and Fehsenfeld, Ref. 26).

4.2.1 Electron Density Disturbance

An illustrative example of the potential influence of ion clustering on thermal instability is provided by consideration of the hydrated-hydronium sequence discussed above. A relatively simple expression for the quasisteady response of the electron density to a disturbance in gas temperature can be derived on the basis of the following assumptions: (1) all hydrated-hydronium ions have approximately the same recombination coefficient which is much larger than that of H_3O^+ at elevated electron temperature; and (2) only the H_3O^+ recombination coefficient depends on electron temperature (Fig. 7). On the basis of these considerations and by using Eq. (12) to relate disturbances in electron temperature and gas temperature, the following equation is obtained,

$$\frac{n_{ek}/n}{T_k/T} \simeq -\frac{1}{2}\left[1 + \frac{\left(\frac{2(1-X_c)k_r^{e\,\hat{}}k_r^e}{1+\hat{\nu}_u+\hat{\nu}_m}\right) + X_c\,\hat{\hat{X}}_c\,k_{r_c}^e}{(1-X_c)k_r^e + X_c\,k_{r_c}^e}\right], \quad \phi = 90\% \quad , \qquad (19)$$

where X_c is the fraction of hydrated ions, $\hat{\hat{X}}_c$ is the fractional derivative of X_c with respect to gas temperature, and k_r^e and $k_{r_c}^e$ are the recombination coefficients for H_3O^+ and $H_3O^+\cdot(H_2O)_n$, respectively. Note that Eq. (19) reduces to Eq. (18) when X_c and δ are zero.

Shown in Fig. 17 are the quantities X_c and $\hat{\hat{X}}_c$ as a function of temperature computed for 1 ppm H_2O at atmospheric density. The corresponding effective value of the recombination coefficient for $T_e \simeq 0.5$ eV is presented in Fig. 18. Note that the transition from $X_c \simeq 1.0$ to $X_c < 10^{-2}$ corresponds to a two order of magnitude decrease in k_r^e which takes place over a relatively small range in temperature. Figure 18 also shows that cluster ions dominate the recombination process when their fraction exceeds only a few percent of the total ion concentration.

Presented in Fig. 19 is the fractional electron density disturbance computed using Eq. (19) and the data of Figs. 17 and 18. In light of the importance of the electron density disturbance on the growth of thermal instability as discussed in Sec. 3, these results are of considerable significance. Figure 19 shows that when either all the ions are clustered ($X_c \sim 1$) or the cluster concentration is very small ($X_c < 10^{-3}$), $(n_{e_k}/n_e)(T_k/T)^{-1}$ is relatively small as desired. However, during the transition from clustered ions to the simple molecular ion H_3O^+ the

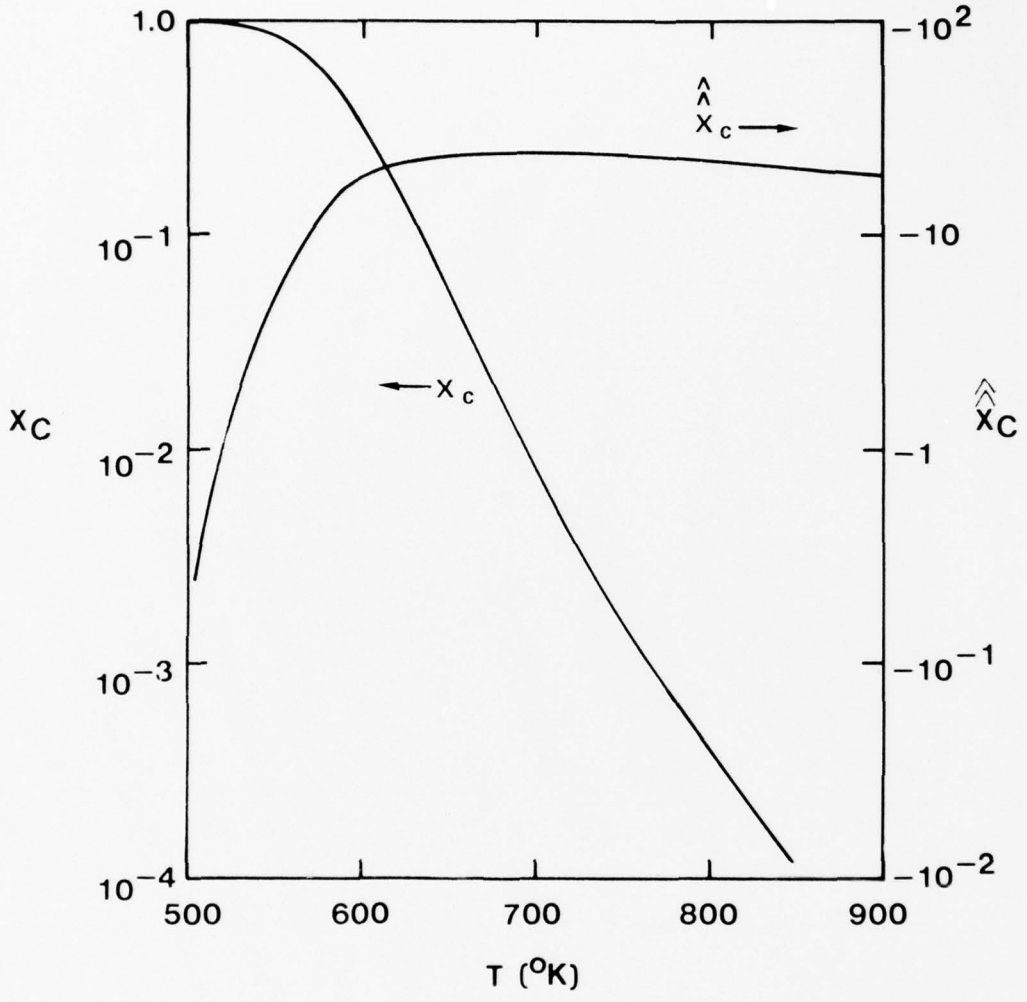

Figure 17. Fractional concentration of hydrated-hydronium ions $[H_3O^+\cdot(H_2O)_n,\ n \geq 1]$, X_c, and the fractional derivative of X_c with respect to T, $\hat{\hat{X}}_c$, for 1 ppm H_2O in an atmospheric density background gas.

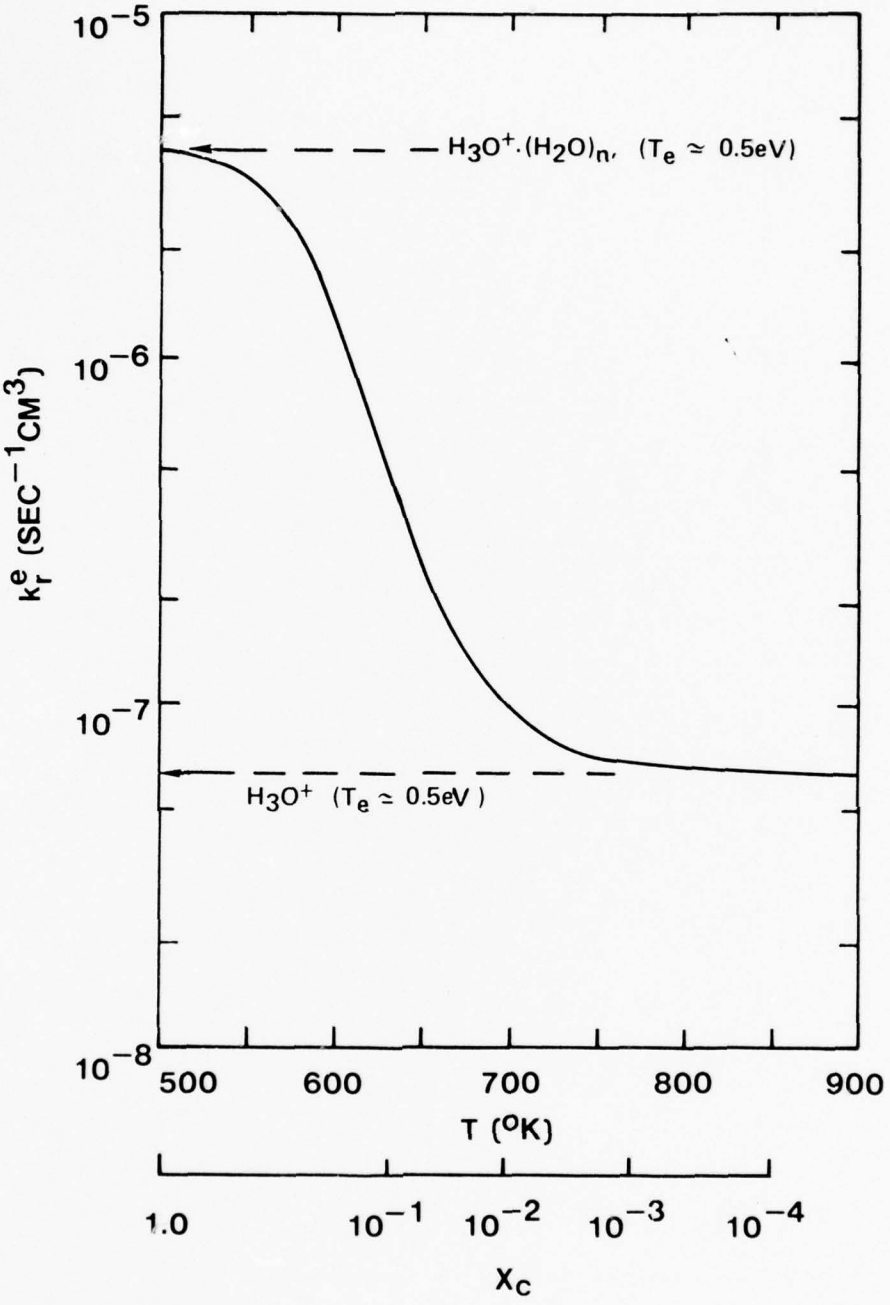

Figure 18. Effective electron recombination coefficient for the $H_3O^+ \cdot (H_2O)_n$ series ions for the conditions of Fig. 17 and an electron temperature of 0.5 eV.

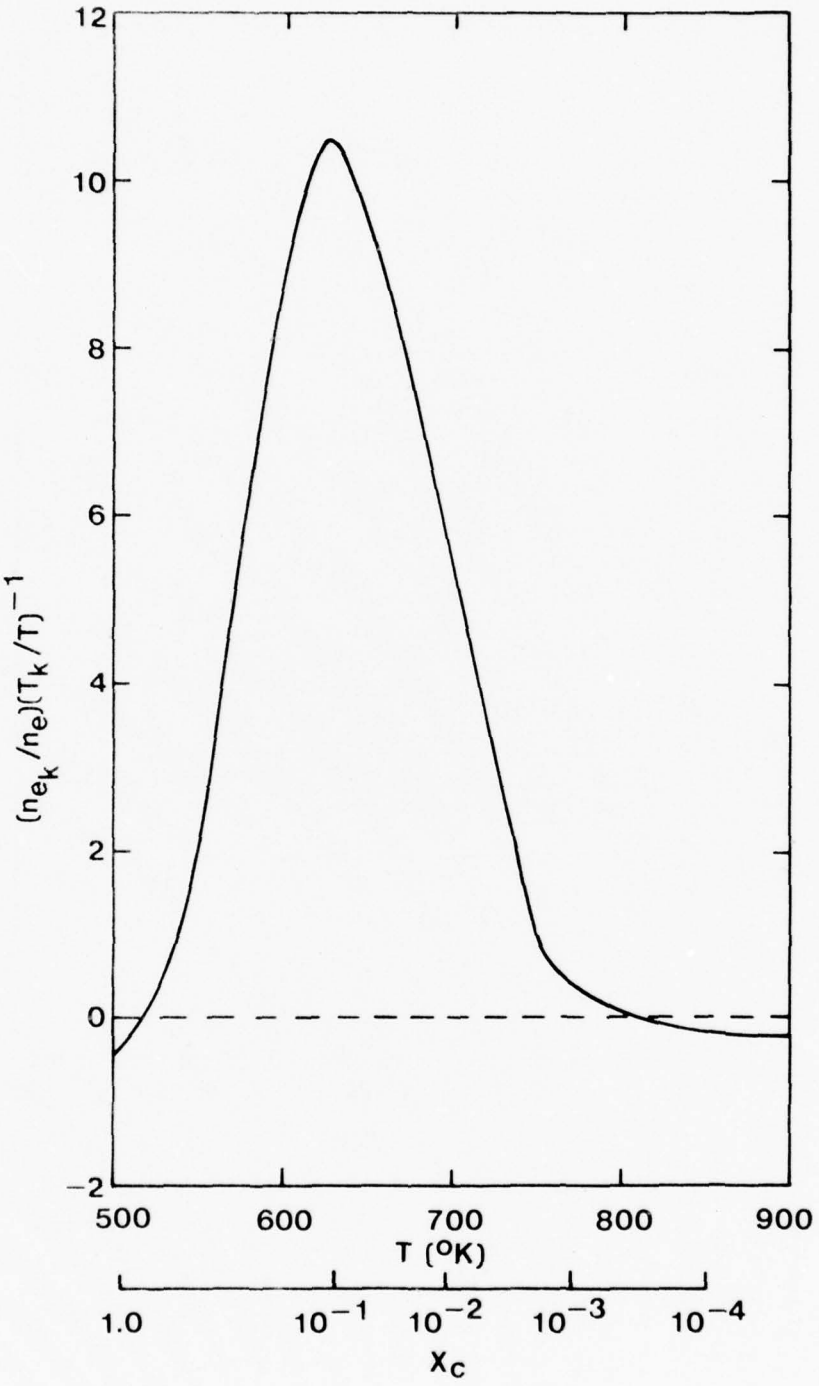

Figure 19. Fractional electron density disturbance relative to a gas temperature disturbance computed for the conditions of Figs. 17 and 18 using the approximate model discussed in Sec. 4.2.1.

magnitude of the fractional electron density disturbance reaches a value typical of a self-sustained discharge, i.e., ~ 10. This is a direct manifestation of the large difference between the recombination coefficient for clustered and molecular ions, coupled with the extreme sensitivity of cluster ion concentration to variations in temperature.

4.2.4 Steady-State and Stability Characteristics

The results presented above show the effect on the magnitude of electron density disturbances of the transition from clustered to molecular ions. For the hydrated-hydronium ion sequence this conversion is effectively completed when the gas translational temperature reaches approximately 750°K (Fig. 18). With the possible exception of the region near boundary layers and/or electrode surfaces, this temperature level is very much higher than that anticipated even in CO_2 lasers. However, the vibrational temperature in both CO and CO_2 lasers exceeds 750°K by a substantial margin; and there is some evidence[29] that increases in vibrational temperature are as effective in cluster ion breakup as a high translational temperature. As an illustration of the potential influence of cluster-to-molecular ion conversion in a vibrationally hot-translationally cold gas, the variation of cluster ion fraction shown in Fig. 17 was assumed to refer to vibrational temperature. An effective recombination coefficient generally similar to that shown in Fig. 18 was then used to compute both the steady state and stability characteristics for the CO EDL conditions used in the analysis of Sec. 3.

Presented in Fig. 20 are computed steady state properties for representative conditions. The most obvious consequence of the complete conversion from clustered to molecular ions is the highly nonuniform axial variation in electron density (and therefore current density). As the effective recombination loss is reduced due to cluster ion disintegration, the electron density rises significantly to the level compatible with the H_3O^+ recombination coefficient. In this connection it is interesting to note that with a few ppm $Fe(CO)_5$ present, attachment loss could become significant as the cluster ion concentration decreases along the flow direction. If this occurred the transition from a recombination dominated to an attachment dominated discharge would evolve spatially as the gas passed through the discharge. Prior analysis has been shown that such a transition should occur in externally sustained CO_2 laser discharges.[1]

Computation of stability characteristics in the present approximation is certainly less accurate than steady state properties, but is qualitatively illustrative nonetheless. Figure 21 presents the approximate thermal instability growth rate and fractional electron density disturbance corresponding to the conditions of Fig. 20. The order of magnitude rise in the growth rate as a consequence of the cluster to molecular ion transition requires no explanation in light of the previous discussion. It is worth pointing out, however, that in this illustrative example conditions were selected so that the transition from clustered to molecular ions

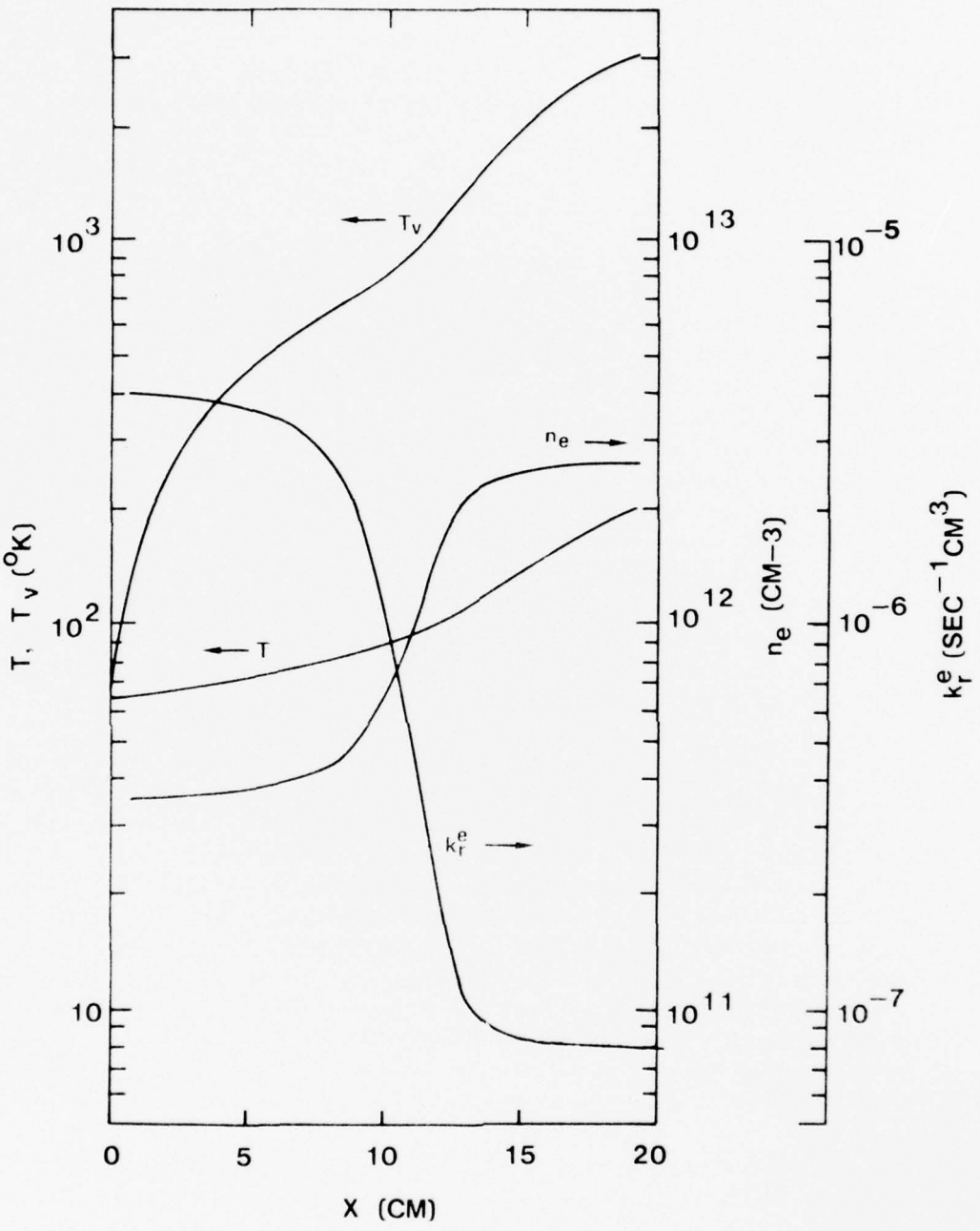

Figure 20. Computed spatial evolution of plasma properties for representative CO laser conditions illustrating the effect of disintegration of hydrated-hydronium ions as the vibrational temperature increases.

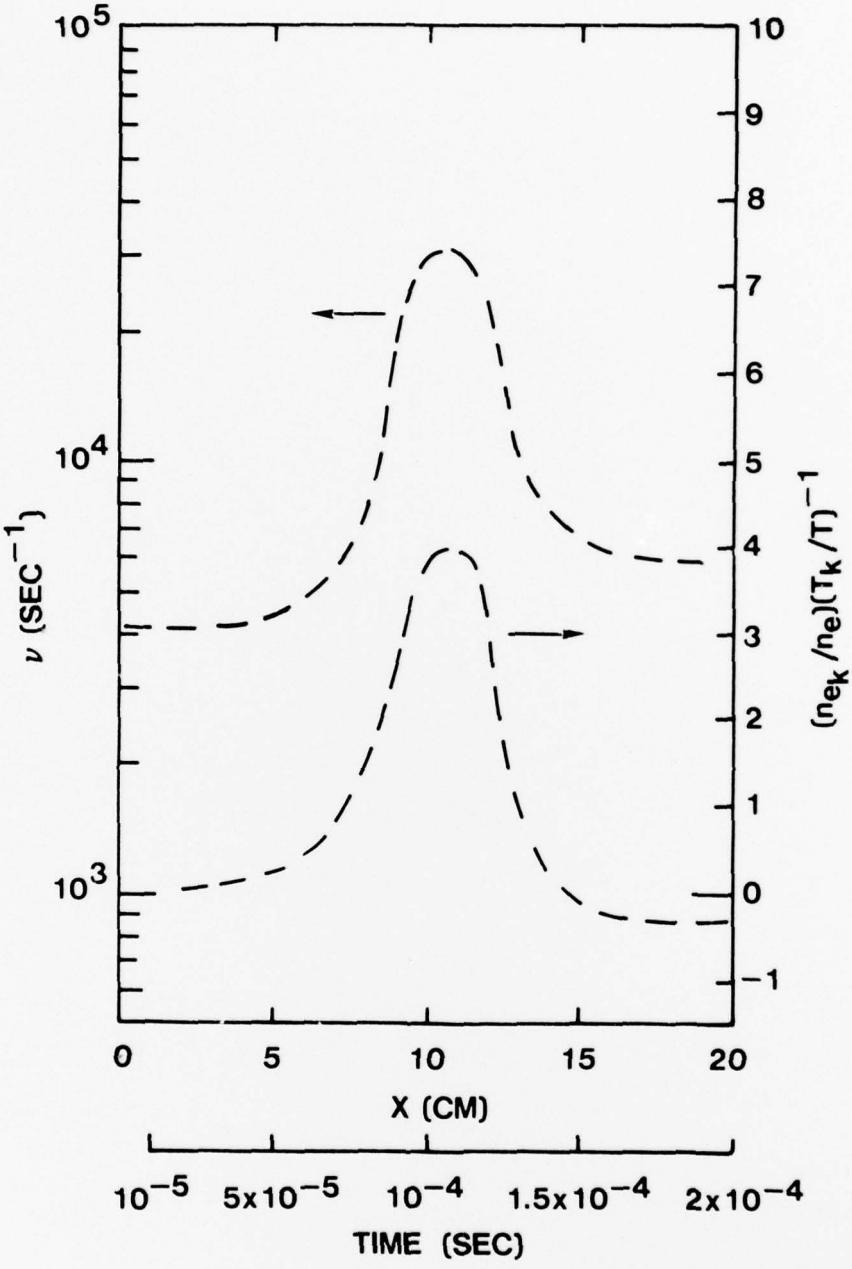

Figure 21. Approximate prediction of the thermal instability growth rate and fractional electron density disturbance corresponding to the conditions of Fig. 20.

was complete. It is entirely possible that under certain conditions cluster ions are not eliminated entirely in spite of the high vibrational energy density. Further, all cluster ions do not have the same recombination coefficient as assumed in this illustration so that spatial and/or temporal rearrangement of cluster ions in response to vibrational temperature change could also lead to variations of the type shown in Figs. 20 and 21.

SECTION 5

SUMMARY

In this investigation the causes of instability in high power CO laser discharges were examined. Emphasis was directed toward specific conditions of importance in Air Force high energy laser technology programs. The principal results of this study are summarized as follows:

(1) For the plasma conditions compatible with average electrical power densities in the kW/cm^3 range, externally sustained CO laser discharges are inherently unstable.

(2) Under the best of circumstances the time characterizing the growth of thermal instabilities will be on the order of 0.1 msec or less at this power density level.

(3) The single most important factor affecting the instability growth rate is the electron loss process; a conclusion also applicable to externally sustained CO_2 laser discharges.

(4) The low temperature-high pressure conditions required for efficient high energy CO laser operation, combined with a very low value of fractional ionization, define a unique environment for volume dominated molecular discharges. Although it is possible to provide a controllable, uniform electron source, the electron loss process is entirely uncontrolled under the conditions typical of present AF experiments. In fact, it is probable that the nature of the electron loss process is dictated by residual impurities.

(5) Determination of the discharge techniques and/or gas additives required to introduce the degree of control over electron loss which is comparable to that of the electron production process requires basic information which is presently unavailable. Until a significantly better understanding of high pressure ion kinetics evolves, glow collapse and/or arcing will continue to be an erratic and unpredictable phenomenon which hinders the development of large scale, high energy electric laser systems.

5.1 Recommendations

This investigation has revealed the critical role played by electron recombination in the growth of thermal instability in externally sustained molecular discharges. Earlier work[1] showed the important effect of negative-ion

attachment-detachment kinetics. It follows that in order to make additional progress in the scaling of both CO and CO_2 laser discharges the following details of positive and negative ion processes must be known for the specific conditions of importance:

(1) The positive and negative ion species typical of atmospheric density laser discharges must be determined experimentally. Special emphasis should be directed toward determination of the effect of variations in neutral and ion translational temperature and of molecule vibrational temperature.

(2) Electron-ion recombination coefficients must be determined for the positive ion species so identified. Special attention should be directed toward determination of the role of molecular ion vibrational temperature.

(3) Detachment rate coefficients for the principle species of negative ions identified should be detemined as a function of translational and vibrational temperature.

(4) The effect of intense i.r. laser radiation in the appropriate wavelength range on positive and negative ion species should be determined.

The promise of efficient, scalable high power molecular lasers relies almost entirely on understanding evolved from a scientific base appropriate only to electric discharges operating in the binary collision regime, i.e., low pressure, diffusion controlled discharges. There is little or no fundamental information relevant to charged particle collision processes under high pressure conditions typical of AF high energy laser experiments. Moreover, laser discharge power loading and dependability of operation continue to be significantly affected by glow collapse and related phenomena, a circumstance which will be further aggravated by closed-cycle operation. The present investigation has shown how and why charged particle kinetic processes in the high pressure regime can significantly influence discharge stability. In addition, the fundamental data which are required to substantially improve basic understanding of high pressure volume dominated discharges have been identified. Thus, the results presented herein should provide the framework within which progress toward solution of laser plasma stability problems can move forward.

REFERENCES

1. Nighan, W. L.: Phys. Rev. 1977 (to be published); also United Technologies Research Center Report R76-921325-6, September 30, 1976.

2. Nighan, W. L.: Stability of High-Power Molecular Laser Discharges. Principles of Laser Plasmas, G. Bekefi (Ed.). J. Wiley & Sons, New York. 1976.

3. Nighan, W. L., and W. J. Wiegand: Phys. Rev. A10, 922. 1974.

4. Haas, R. A.: Phys. Rev. A8, 1017. 1973.

5. Shields, H., A. L. S. Smith and E. Norris: J. Phys. D: Appl. Phys. 9, 1587. 1976.

6. Hall, R. J., and A. C, Eckbreth: IEEE J. Quant. Electron. QE-10, 580. 1974.

7. Horton, R. L., J. L. Franklin and B. Mazzeo: J. Chem. Phys. 62, 1730. 1975.

8. Ellis, H. W., R. Y. Pai, I. R. Gatland and E. W. McDaniel: J. Chem. Phys. 64, 3935, 1976.

9. Biondi, M. A.: Recombination. Principles of Laser Plasmas, G. Bekefi (Ed.), J. Wiley & Sons, New York. 1976.

10. Center, R. E.: J. Appl. Phys. 44, 3528. 1973.

11. Center, R. E.: IEEE J. Quant. Electron QE-10, 208. 1974.

12. Parr, J. E. and J. L. Morruzzi: Proc. of the 10th Intl. Conf. on Phenomena in Ionized Gases. Oxford 1971.

13. Douglas-Hamilton, D. H.: J. Chem. Phys. 58, 4820. 1973.

14. Meyer, T. W., J. D. Hines, and P. D. Tannen: Electron-Ion Recombination in Gas Mixtures. Presented at the 29th Annual Gaseous Electronics Conference. October 19-22, 1976. Cleveland, Ohio.

15. Daiber, J., H. M. Thompson and T. J. Falk: IEEE J. Quant. Electron. QE-12, 686, 1976.

16. Keren, H., P. Avivi, and F. Dothen: IEEE J. Quant. Electron. QE-12 58. 1976.

17. Morgan, W. L. and E. R. Fisher: Private Communication.

REFERENCES (Cont'd)

18. McKeown, M., and M. W. Siegel: American Laboratory 1, 89. 1975.

19. Siegel, M., and M. C. McKeown: J. of Chromatography 122, 397. 1976.

20. Kadlecek, J.: Positive Ions of Atmospheric Importance. PhD Dissertation, State Univ. of N.Y. at Albany. 1974. (Unpublished).

21. Fehsenfeld, F. C., M. Moseman, and E. E. Ferguson: J. Chem. Phys. 55, 2115. 1971.

22. Fehsenfeld, F. C., M. Moseman and E. E. Ferguson: J. Chem. Phys. 55, 2120. 1971.

23. Ferguson, E. E.: Rev. Geophys. Space Phys. 12, 703. 1974.

24. Good, A., D. A. Durden, and P. Kebarle: J. Chem. Phys. 52, 212. 1970.

25. Kebarle, P., S. K. Searles, A. Zolla, J. Scarborough and M. Arshadi: J. Am. Chem. Soc. 89, 6393. 1967. Also Cunningham, A. J., J. D. Payzant and P. Kebarle: J. Am. Chem. Soc. 96, 7627. 1972.

26. McFarland, M., D. L. Albritton and F. C. Fehsenfeld: (Unpublished).

27. Leu, M. T., M. A. Biondi and R. Johnsen: Phys. Rev. A7, 292. 1973.

28. R. Johnsen: Private Communication.

29. Burke, R. R.: Shock Layer Measurements of Decomposition Reactions of Water Cluster Ions. COSPAR Symposium of D and E Region Ion Chemistry. July 6-8, 1971. University of Illinois Aeronomy Laboratory Report UILU-ENG-72-2503 (C. F. Sechrist and M. A. Getter, Editors).

APPENDIX

CLUSTER ION DATA COMPILATION

This appendix countains a summary of rate coefficients for the formation and recombination of certain cluster ion species which may be of importance in high power CO and CO_2 electric discharge laser applications. In some cases cluster bond energies and reaction temperature dependences are also given for purposes of comparison.

It should be emphasized that the cluster ion formation data in Sec. I of this appendix were all obtained at low temperature ($\lesssim 300^{o}K$) under conditions of thermodynamic equilibrium, i.e., $T_e = T_v = T$. Also, in many of the measurements leading to the recombination data in Sec. II the degree of vibrational excitation of the ions was unknown.

Unfortunately there are no data of this type available for discharge conditions representative of high power CO and CO_2 laser discharges. In view of the discussion in Secs. 3 and 4 of this report it is clear that there exists a significant gap in the CO/CO_2 data base which could be of considerable importance.

CLUSTER ION PROCESSES

Reaction	Rate Coefficient[a]	Reference	Notes[b]
I. Cluster Ion Formation			
A. $CO^+ \cdot (CO)_n$ Series			
(1) $CO^+ + 2CO \rightarrow CO^+ \cdot CO + CO$	1.07(-28)T = 174°K	1	$\Delta E \sim 1.2$eV, $\lvert\hat{\hat{k}}\rvert < 1$
	7.6(-29) T = 200	1	" "
	1.1(-28) T = 280	1	" "
	1.1(-28) T = 300	2	" "
(2) $CO^+ \cdot CO + 2CO \rightarrow CO^+ \cdot (CO)_2 + CO$	1.06(-29)T = 174°K	1	$\Delta E \sim 2.1$eV, $\hat{\hat{k}} \sim -2$
	5.58(-30)T = 200	1	" "
	3.86(-30)T = 280	1	" "
(3) $CO^+ \cdot (CO)_2 + 2CO \rightarrow CO^+ \cdot (CO)_3 + CO$	6.06(-30)T = 174°K	1	$\Delta E \sim 0.4$eV

Reaction	Rate Coefficient	Reference	Notes
B. $O_2^+ \cdot (O_2)_n$ Series[c]			
(4) $O_2^+ + 2O_2 \rightarrow O_2^+ \cdot O_2 + O_2$	2.6(-30)T = 300°K	3	$\Delta E \sim 0.45$, $\hat{\hat{k}} = -3.2$, T < 300°K
(5) $O_2^+ + O_2 + He \rightarrow O_2^+ \cdot O_2 + He$	2.4(-30)T = 200°K 3.1(-29)T = 82°K	4,5 6,5	" "
(6) $O_2^+ + O_2 + Kr \rightarrow O_2^+ \cdot O_2 + Kr$	8.3(-30)T = 180°K	7	"
(7) $O_2^+ \cdot O_2 + 2O_2 \rightarrow O_2^+ \cdot (O_2)_2 + O_2$	7.0(-32)T = 300°K	3	$\Delta E \sim 0.28$, $\hat{\hat{k}} = -5.1$, T < 300°K
(8) $O_2^+ \cdot (O_2)_2 + 2O_2 \rightarrow O_2^+ \cdot (O_2)_3 + O_2$	2.5(-29)T = 90°K	3	$\Delta E \sim 0.11$
(9) $O_2^+ \cdot O_2 + O_2 + He \rightarrow O_2^+ \cdot (O_2)_2 + He$	5.0(-30)T = 80°K	4,5	$\Delta E \sim 0.28$
C. Hydrated Ions[d]			
(10) $CO^+ + H_2O + CO \rightarrow CO^+ \cdot H_2O + CO$	1.56(-26)T = 174°K	1	$\Delta E \sim 2.0$eV
(11) $CO^+ \cdot CO + H_2O \rightarrow CO^+ \cdot H_2O + CO$	9.9(-10) T = 174°K 1.1(-9) T = 200 1.6(-9) T = 280	1 1 1	$\Delta E \sim 2.0$eV, $\hat{\hat{k}} \sim 1$ " " " "
(12) $CO^+ \cdot H_2O + H_2O \rightarrow H_3O^+ + HCOO$	3(-10) T = 174-280°K	1	$\Delta E \sim 1.0$eV
(13) $CO^+ + H_2O \rightarrow HCO^+ + OH$	2.8(-10) T = 174°K 2.3(-10) T = 200 3.9(-10) T = 280	1 1 1	$\Delta E \sim 1.0$eV " "
(14) $O_2^+ + H_2O + M \rightarrow O_2^+ \cdot H_2O + M$	0.9(-28), M = He, T = 295°K 2.8(-28), N_2 2.0(-28), A_r	8	$\Delta E \sim 0.95$ " "
(15) $O_2^+ \cdot O_2 + H_2O \rightarrow O_2^+ \cdot H_2O + O_2$	2.2(-9), T = 295	8	"
(16) $O_2^+ \cdot H_2O + H_2O \rightarrow H_3O^+ \cdot OH + O_2$ $\rightarrow H_3O^+ + OH + O_2$	1.9(-9), T = 295°K < 3(-10)	8	

CLUSTER ION PROCESSES (Cont'd)

Reaction	Rate Coefficient	Reference	Notes
(17) $NO^+ + H_2O + M \rightarrow NO^+ \cdot H_2O + M$	3.6(-29) M = He, T = 295°K 7.8(-29) A_r 1.6(-28) N_2 1.6(-28) NO	9	
(18) $NO^+ \cdot H_2O + H_2O + M \rightarrow NO^+ \cdot (H_2O)_2 + M$	3.0(-28) M = He, T = 295°K 8.0(-28) A_r 1.0(-27) N_2 1.1(-27) NO	9	
(19) $NO^+ \cdot (H_2O)_2 + H_2O + M \rightarrow NO^+ \cdot (H_2O)_3 + M$	4.0(-28) M = He, T = 295°K 1.5(-27) A_r 2.0(-27) N_2 1.9(-27) NO	9	
(20) $NO^+ \cdot (H_2O)_3 + H_2O \rightarrow H_3O^+ \cdot (H_2O)_2 + HNO_2$	8.0(-11), T = 295°K	9	$\Delta E \sim .97$eV
(21) $N_2^+ \cdot N_2 + H_2O \rightarrow H_2O^+ + 2N_2$	1.9(-9), T = 300°K	10	
(22) $H_2O^+ + H_2O \rightarrow H_3O^+ + OH$	1.8(-9)	10	
(23) $H_3O^+ + H_2O + N_2 \rightleftarrows H^+ \cdot (H_2O)_2 + N_2$	3.4(-27), (7.0(-26))	10	$\Delta E \sim 1.57$eV
(24) $H^+ \cdot (H_2O)_2 + H_2O + N_2 \rightleftarrows H^+ \cdot (H_2O)_3 + N_2$	2.3(-27), (7.0(-18))	10	$\Delta E \sim .97$eV
(25) $H^+ \cdot (H_2O)_3 + H_2O + N_2 \rightleftarrows H^+ \cdot (H_2O)_4 + N_2$	2.4(-27), (4.0(-14))	10	$\Delta E \sim .74$eV
(26) $H^+ \cdot (H_2O)_4 + H_2O + N_2 \rightleftarrows H^+ \cdot (H_2O)_5 + N_2$	0.9(-27), (6.0(-12))	10	$\Delta E \sim .67$eV

CLUSTER ION PROCESSES (Cont'd)

Reaction	Rate Coefficient	Reference	Notes
D. Mixed Clusters			
(27) $O_2^+ \cdot O_2 + N_2 + H_e \rightarrow O_2^+ \cdot O_2 \cdot N_2 + H_e$	$1.0(-29)T = 80^oK$	4,5	$\Delta E \sim 0.1eV$
(28) $O_2^+ + CO_2 + H_e \rightarrow O_2^+ \cdot CO_2 + H_e$	$2.3(-29)T = 200^oK$	4,5	$\Delta E \sim 0.70$
(29) $O_2^+ + N_2 + H_e \rightarrow O_2^+ \cdot N_2 + H_e$	$1.9(-29)T = 80^oK$	4,5	$\Delta E \sim 0.2$
(30) $O_2^+ + N_2O + H_e \rightarrow O_2^+ \cdot N_2O + H_e$	$5.2(-29)T = 200^oK$	4,5	$\Delta E \sim 0.9$
(31) $O_2^+ \cdot N_2 + N_2 + H_e \rightarrow O_2^+ \cdot (N_2)_2 + H_e$	$1.0(-29)T = 80^oK$	4,5	$\Delta E \sim 0.1$
(32) $NO^+ + 2CO_2 \rightarrow NO^+ \cdot CO_2 + CO_2$	$2.4(-29)T = 300^oK$	11	
(33) $NO^+ + 2N_2 \rightarrow NO^+ \cdot N_2 + N_2$	$2.0(-31)T = 300^oK$	11	
(34) $NO^+ + 2N_2 \rightarrow NO^+ \cdot N_2 + N_2$	$8.0(-30)T = 130^oK$	12	
(35) $NO^+ + 2O_2 \rightarrow NO^+ \cdot O_2 + O_2$	$9.0(-32)T = 300^oK$	11	
E. Other Ions			
(36) $C^+ + O_2 \rightarrow CO^+ + O$	$1.1(-9)T = 300^oK$	13,14	
(37) $C^+ + CO_2 \rightarrow CO^+ + CO$	$1.9(-9)T = 300^oK$	13,14	
(38) $CO_2^+ + 3CO_2 \rightarrow CO_2^+ \cdot CO_2 + 2CO_2$	$1.0(-43)T = 300^oK$	15,16	
(39) $HCO^+ + H_2O \rightarrow H_3O^+ + CO$	$1.28(-9)T = 174$	1	
(40) $O_2^{+*} + CO \rightarrow CO^+ + O_2$ $CO_2^+ + O$ $O_2^+ + CO$	$2.0(-10)T = 300^oK$	17	
(41) $O_2^{+*} + CO_2 \rightarrow CO_2^+ + O_2$ $O_2^+ + CO_2$	$9.0(-10)T = 300^oK$	17	

CLUSTER ION PROCESSES (Cont'd)

Reaction	Rate Coefficient	Reference	Notes
II. Electron-Ion Recombination			
A. CO^+ Initial Core			
(1) $e + CO^+$	$3.9(-7)T_e = T = 775^oK$	18	$\hat{k}_r^e = -.58$
$e + CO^+ \cdot CO$	$1.0(-7)T_e = T = 0.8eV$	19	$\hat{k}_r^e = -1.6, 0.1 < T_{e(eff)} < 1.0$ eV
B. O_2^+ Initial Core			
(2) $e + O_2^+$	$0.8(-7)T_e = 1000^oK$	20	$\hat{k}_r^e = -0.56, T_e > 1000^oK$
(3) $e + O_2^+$	$3.5(-7)T_e = T = 180^oK$	7	
(4) $e + O_2^+ \cdot O_2$	$1.8(-6)T_e = 180^oK$	7	
C. Hydronium Series			
(5) $e + H_3O^+$	$1.0(-6)T_e = 540^oK$	21,22	$\hat{k}_r^e = -1, 1000^oK < T_e < 5000^oK$ $\hat{k}_r^e < -1, T_e > 5000^oK$
(6) $e + H_3O^+ \cdot (H_2O)$	$2.0(-6)T_e = T = 540^oK$	21	$\hat{k}_r^e \sim 0$
	$2.2(-6)T_e = 415^oK$	21	"
(7) $e + H_3O^+ \cdot (H_2O)_2$	$4.0(-6)T_e = 540^oK$	21	"
	$4.2(-6)T_e = 415$	21	"
	$3.8(-6)T_e = 300$	21	"
(8) $e + H_3O^+ \cdot (H_2O)_3$	$4.9(-6)T_e = 300^oK$	21	"
(9) $e + H_3O^+ \cdot (H_2O)_4$	$6.0(-6)T_e = 205^oK$	21	"
(10) $e + H_3O^+ \cdot (H_2O)_5$	$7.5(-6)T_e = 205^oK$	21	"
(11) $e + H_3O^+ \cdot (H_2O)_6$	$\lesssim 1.0(-5)T_e = 205^oK$	21	"

CLUSTER ION PROCESSES (Cont'd)

Reaction	Rate Coefficient	Reference	Notes
D. Ammonium Series			
(12) $e + NH_4^+$	$1.3(-6)T_e = T = 410^oK$ $1.5(-6)T_e = 300^oK$ $5.2(-6)T_e = 200^oK$	23	
(13) $e + NH_4^+\cdot(NH_3)$	$2.8(-6)T_e = 300^oK$	23	$\hat{k}_r^e = -0.15$
(14) $e + NH_4^+\cdot(NH_3)_2$	$2.7(-6)T_e = 300^oK$	23	$\hat{k}_r^e = -0.05$
(15) $e + NH_4^+\cdot(NH_3)_{3,4}$	$3.0(-6)T_e = 300^oK$	23	

---

a Rate coefficients for two-body processes are expressed in $sec^{-1}cm^3$; three-body processes, $sec^{-1}cm^6$; and four-body processes, $sec^{-1}cm^9$. For three-body reactions the product $k[M]$ saturates at a value of approximately $2\text{-}5 \times 10^{-9}$ $sec^{-1}cm^3$ as the pressure increases.

b ΔE represents the exothermicity of the indicated reactions. In the case of cluster ion formation ΔE reflects the energy required to remove the last neutral molecule added. Thus, ΔE provides an approximate measure of the thermal stability of the cluster ion complex. Generally, the energies ΔE and electron and gas temperature dependence of reactions as reflected by $\hat{k}_r^e$ and $\hat{k}$ are much less reliable than the magnitude of the reaction rate coefficients.

c See Ref. 24 for the equilibrium constants for the $O_2^+\cdot(O_2)_n$ series.

d See Ref 25 for the equilibrium constants for the $H^+\cdot(H_2O)_n$ series.

e The assumption that the ion species in the measurements of Ref. 19 was $CO^+\cdot CO$ as indicated here is questionable. See the discussion of Sec. 4.

REFERENCES FOR APPENDIX

1. Horton, R. L., J. L. Franklin and B. Mazzeo: J. Chem. Phys. 62, 1739. 1975.

2. Schummers, J. H., G. M. Thomson, D. R. James, E. Graham, I. R. Gatland, and E. W. McDaniel: Phys. Rev. A 7, 689. 1973.

3. Payzant, J. D., A. J. Cunningham and P. Kebarle: J. Chem. Phys. 59, 5615. 1973.

4. Adams, N. G., D. K. Bohme, D. B. Dunkin, F. C. Fehsenfeld, E. E. Ferguson: J. Chem. Phys. 52, 3133. 1970.

5. Good, A.: Int. J. Mass Spectrom, Ion Phys. 10, 379. 72/73.

6. Bohme, D. K., D. B. Dunkin, F. C. Fehsenfeld, E. E. Ferguson: J. Chem. Phys. 51, 863. 1969.

7. Plumb, I. C., D. C. Smith, N. G. Adams: J. Phys. B: Atomic and Mol. Phys. 5, 1762. 1972.

8. Fehsenfeld, F. C., M. Moseman and E. E. Ferguson: J. Chem. Phys. 55, 2115. 1971.

9. Fehsenfeld, F. C., M. Moseman and E. E. Ferguson: J. Chem. Phys. 55, 2120. 1971.

10. Good, A., D. A. Durden and P. Kebarle: J. Chem. Phys. 52, 212. 1970.

11. Heimerl, J. M. and J. A. Vanderhoff: J. Chem. Phys. 60, 4362. 1974.

12. Johnsen, R., C. M. Huang and M. A. Biondi: J. Chem. Phys. 63, 3374. 1975.

13. Fehsenfeld, F. C., A. L. Schmeltekopf and E. E. Ferguson: J. Chem. Phys. 45, 23. 1966.

14. Rutherford, J. A. and D. A. Vroom: J. Chem. Phys. 64, 3057. 1976.

15. Schildcrout, S. M., J. G. Collins and J. L. Franklin: J. Chem. Phys. 52, 5767. 1970.

16. Ellis, H. W., R. Y. Pai, I. R. Gatland and E. W. McDaniel: J. Chem. Phys. 64, 3935. 1976.

17. Lindinger, W., D. L. Albritton, M. McFarland, F. C. Fehsenfeld, A. L. Schmeltekopf: J. Chem. Phys. 62, 410. 1975.

18. Mentzoni, M. H. and J. Donohoe: Can. J. Phys. 47, 1789. 1969.

19. Center, R. E.: J. Chem. Phys. 58, 5230. 1973.

20. Bardsley, J. N. and M. A. Biondi: Dissociative Recombination. In Advances In Atomic and Molecular Physics. Vol. 6, Academic Press, New York. 1970. Also, M. A. Biondi: Recombination. In Principles of Laser Plasmas. G. Bekefi (Ed.), John Wiley and Sons, New York. 1976.

21. Leu, M. T., M. A. Biondi and R. Johnsen: Phys. Rev. A7, 292. 1973.

22. Heppner, R. A., F. L. Walls, W. T. Armstrong and G. H. Dunn: Phys. Rev. A 13, 1000. 1976.

23. Huang, C. M., M. A. Biondi and R. Johnsen: Phys. Rev. A14, 984. 1976.

24. Conway, D. C. and G. S. Janik: J. Chem. Phys. 53, 1859. 1970.

25. Cunningham, A. J., J. D. Payzant and P. Kebarle: J. Am. Chem. Soc. 94, 7627. 1972.

*U.S.Government Printing Office: 1977 — 757-001/74